Supporting information

Multifunctional assistant acceptor modulated pyrenyl phenanthrimidazole derivatives for highly efficient blue and host-sensitized OLEDs

Jayaraman Jayabharathi*, Jagathratchagan Anudeebhana, Venugopal Thanikachalam, Sekar Sivaraj

Department of Chemistry, Material Science Lab, Annamalai University, Annamalai nagar, Tamilnadu- 608 002, India

Contents

SI-I. (i) General information

All the reagents and solvents were purchased from commercial sources and used as received. The emitters were subjected to sublimation to enhance the purity before photoluminescence and electroluminescence investigations. ^{1}H and ^{13}C NMR spectra were recorded at room temperature on Bruker 400 spectrometer in CD_2Cl_2. The mass spectra were recorded on Agilent LCMS VL SD. The UV-Vis spectra were recorded on Lambda 35 PerkinElmer (solution)/ Lambda 35 spectrophotometer (RSA-PE-20) (film). The emission spectra were recorded with Perkin Elmer LS55 spectrometer and quantum yield was measured with fluorescence spectrometer (Model-F7100 with integrating sphere). The decomposition temperature (T_d) and glass transition temperature (T_g) were measured with NETZSCH (DSC-204) (10° C min^{-1}; N_2 atmosphere), respectively. Fluorescence lifetime was estimated by time correlated single-photon counting (TCSPC) method on Horiba Fluorocube-01-NL lifetime system: nano LED is an excitation source with TBX-PS is detector; DAS6 software was employed to analyse the decay by reconvolution method. Oxidation potential were measured from potentiostat electrochemical analyzer (CHI 630A) in dichloromethane at a scan rate of 100 mV s^{-1}, platinum wire as auxiliary electrode, glass carbon disk as working electrode and Ag/Ag^{+} as reference electrode. Ferrocene was used as an internal standard with HOMO of -4.80 eV and 0.1M tetrabutylammoniumperchlorate in CH_2Cl_2 as supporting electrolyte. All density functional theory (DFT) calculations were carried out using Gaussian 09 package [1] and Multiwfn [1]. The ground-state (S0) geometries in the gas phase were initially optimized at the level of B3LYP/6-31G (d, p), a commonly used level for the precise geometry optimization. Then, geometry optimization of S1 and excited-state properties based on S1 geometries were studied using time-dependent DFT (TD-DFT) at the same level. The natural transition orbitals (HONTOs and LUNTOs) with hole-particle contribution, transition density matrix and overlap integral have been studied in detail.

(ii) OLEDs fabrication and measurement

ITO glass (resistance 20 Ω/sq) were cleaned with acetone, deionized water and isopropanol and dried (120 ^{o}C) followed by UV-zone treatment (20 min) and transferred into deposition system. The devices were fabricated by multiple source beam deposition method (vacuum pressure - 4 × 10^{-5} mbar). Evaporation rate of 2-4 Å s^{-1} (organic materials) and 0.1 and4 Ås^{-1} for LiF and metal electrodes were applied, respectively. The thickness of each decomposition layer was monitored with quartz crystal thickness monitor. The EL measurement was recorded with USB-650-VIS-NIR spectrometer (Ocean Optics, Inc, USA). The current density-voltage-luminance (J-V-L) characteristics were performed using source meter (Keithley 2450) equipped with LS-110 light intensity meter. The external quantum efficiency was determined from luminance, current density and EL spectrum assuming Lambertian distribution.

(iii) Synthesis of emissive materials

Synthetic route of the emissive materials was outlined in Scheme S1.

(a) 4-(6,9-dibromo-2-(pyren-1-yl)-1H-phenanthro[9,10-d]imidazol-1-yl)naphthalene-1-carbonitrile (BrPPINCN)

The intermediate, BrPPINCN was synthesized by refluxing 3, 6-dibromophenanthrene-9, 10-dione (8.2 mmol), pyrene-1-carbaldehyde (12.3 mmol), 4-formyl-1-naphthonitrile (50 mmol) and ammonium acetate (101.8 mmol) in glacial acetic acid (40 ml) for 12 h (120°C; N_2). The yellow solution was poured into ethanol and the separated solid was washed with methanol and dried. The crude was purified by column chromatography. Yield: 76 %. ^{1}H NMR (400 MHz, $CDCl_3$), δ (ppm): 7.36-7.58 (m, 4H), 7.64-7.96 (m, 7H), 8.00-8.14 (m, 4H), 8.48-8.73 (t, 4H), 8.94 (d, 2H). ^{13}C NMR (400 MHz, $CDCl_3$), δ (ppm): 114.8, 116.8, 120.7, 122.0, 123.2, 124.0, 126.4, 127.8, 128.2, 129.0, 131.8, 133.0, 135.2, 148.2.

(b) 4-(2-(pyren-1-yl)-1H-phenanthro[9,10-d]imidazol-1-yl)naphthalene-1-carbonitrile (PPINCN)

The synthetic procedure adopted was similar as that described for BrPPINCN. Yield: 80 %. ^{1}H NMR (400 MHz, $CDCl_3$), δ (ppm): 7.32 (d, 2H), 7.48-7.56 (m, 6H), 7.60-7.96 (m, 6H), 8.05 (d, 2H), 8.20-8.46 (t, 5H), 8.78 (d, 2H) (Plate S1). ^{13}C NMR (100 MHz, $CDCl_3$), δ (ppm): 109.1, 115.0, 119.8, 122.0, 123.4, 126.0, 127.2, 128.0, 129.1, 131.2, 132.0, 134.8, 139.0, 149.6. HR-MS ($C_{42}H_{23}N_3$): m/z. 571.67 [M+], Calcd. 571.73. Anal. Cacld (%) for C, 88.50; H, 4.07; N, 7.38. Found: C, 88.45; H, 4.01; N, 7.31.

(c) 4-(6,9-bis(4-(1,2,2-triphenylvinyl)phenyl)-2-(pyren-1-yl)-1H-phenanthro[9,10-d]imidazol-1-yl)naphthalene-1-carbonitrile (PPINCN-TPE)

A mixture of BrPPINCN (2mmol), (4-(2,2-diphenylvinyl)phenyl)boronic acid (6 mmol), $Pd(PPh_3)_4$ (0.4 mmol) and K_2CO_3 (6 mmol) in mixed solvents toluene, ethanol and water (8:1:1) was refluxed for 12 h. After cooling, the mixture was poured into water and extracted twice with dichloromethane and dried. The residue was purified by silica gel column chromatography (petroleum ether/DCM, 1:1) and yellow solid of PPINCN-TPE was obtained. Yield: 69%. ^{1}H NMR (400 MHz, $CDCl_3$), δ (ppm): 7.11 (s, 2H), 7.20 (s, 2H), 7.28-7.39 (m, 7H), 7.40-7.52 (m, 8H), 7.60-7.65 (m, 6H), 7.70 (d, 4H), 7.80 (d, 3H), 7.92-8.00 (m, 8H), 8.05-8.10 (m, 9H), 8.1-8.20 (t, 8H), 8.93 (s, 2H) (Plate S2). ^{13}C NMR (100 MHz, $CDCl_3$, δ (ppm): 109.0, 112.8, 117.6, 119.8, 121.7, 123.1, 124.8, 125.6, 126.8, 127.3, 127.8, 128.0, 129.0, 129.2, 131.3, 132.8, 133.6, 134.0, 135.0, 142.08, 144.6, 146.7, 149.4. HR-MS ($C_{94}H_{59}N_3$): m/z. 1232.51 [M+], Calcd. 1232.26. Anal. Cacld (%) for C, 91.50; H, 4.83; N, 3.14. Found: C, 91.45; H, 4.79; N, 3.08.

(d) 4-(6,9-bis(4-(9H-carbazol-9-yl)phenyl)-2-(pyren-1-yl)-1H-phenanthro[9,10-d] imidazol-1-yl)naphthalene-1-carbonitrile (PPINCN-Cz)

The synthetic procedure adopted was similar as that described for PPINCN-TPE by using (4-(9H-carbazol-9-yl)phenyl)boronic acid. Yield: 52%. ^{1}H NMR (400 MHz, $CDCl_3$), δ

(ppm): 6.90-7.02 (m, 7H), 7.10-7.25 (m, 9H), 7.31-7.42 (m, 7H), 7.50-7.61 (m, 7H), 7.80 (d, 2H), 7.93 (d, 2H), 8.01-8.16 (m, 9H), 9.15 (s, 2H) (Plate S3). ^{13}C NMR (100 MHz, $CDCl_3$), δ (ppm): 110.8, 111.6, 113.2, 115.0, 116.0, 118.2, 120.6, 123.9, 124.2, 126.8, 127.0, 128.2, 129.0, 131.8, 132.6, 133.1, 134.0, 136.8, 137.0, 139.3, 142.3. HR-MS ($C_{78}H_{45}N_5$): m/z. 1053.24 [M+], Calcd: 1053.17. Anal. Cacld (%) for C, 89.30; H, 4.39; N, 6.76. Found: C, 88.97; H, 4.28; N, 6.60.

Scheme S1. Synthetic route of emissive materials.

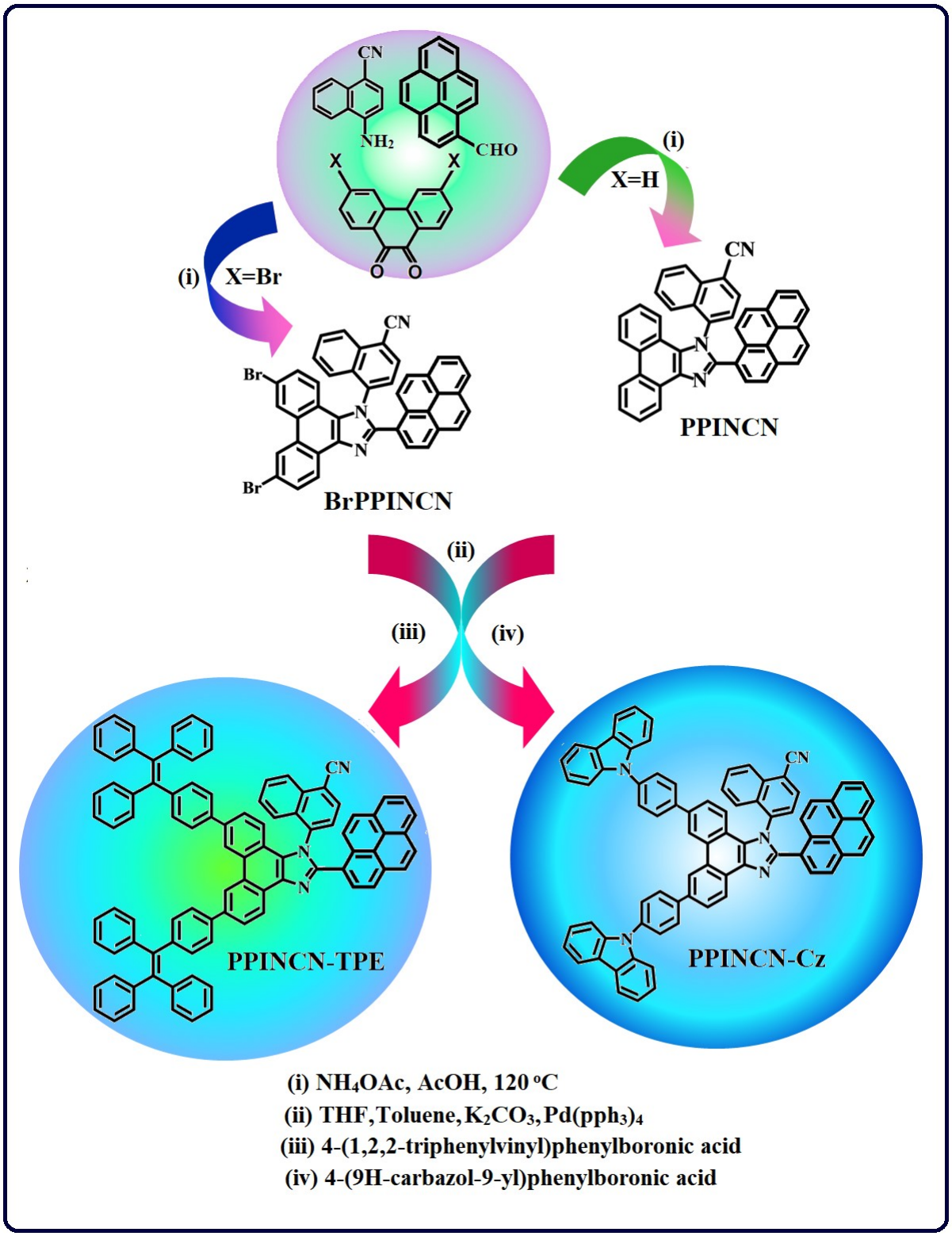

Plate S1. ^{1}H NMR spectrum of 4-(2-(pyren-1-yl)-1H-phenanthro[9,10-d]imidazol-1-yl)naphthalene-1-carbonitrile (PPINCN).

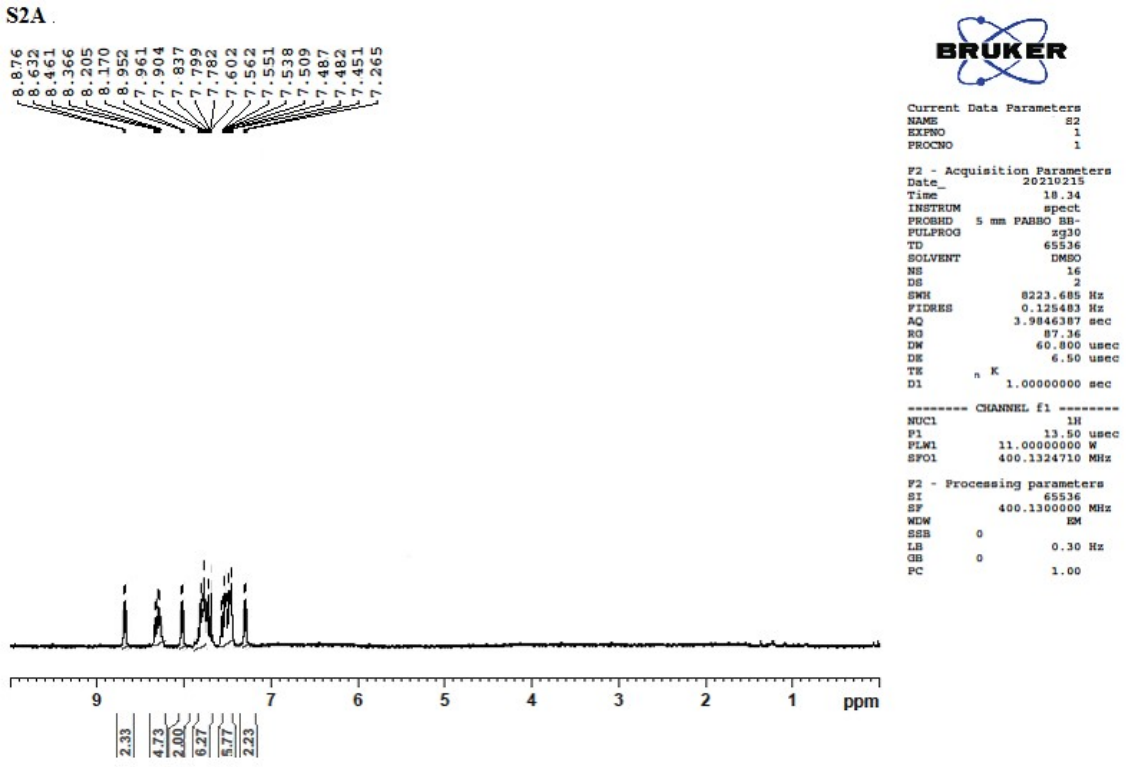

Plate S2. ^{1}H NMR spectrum of 4-(6,9-bis(4-(1,2,2-triphenylvinyl) phenyl)-2-(pyren-1-yl)-1H-phenanthro[9,10-d]imidazol-1-yl)naphthalene-1-carbonitrile (PPINCN-TPE).

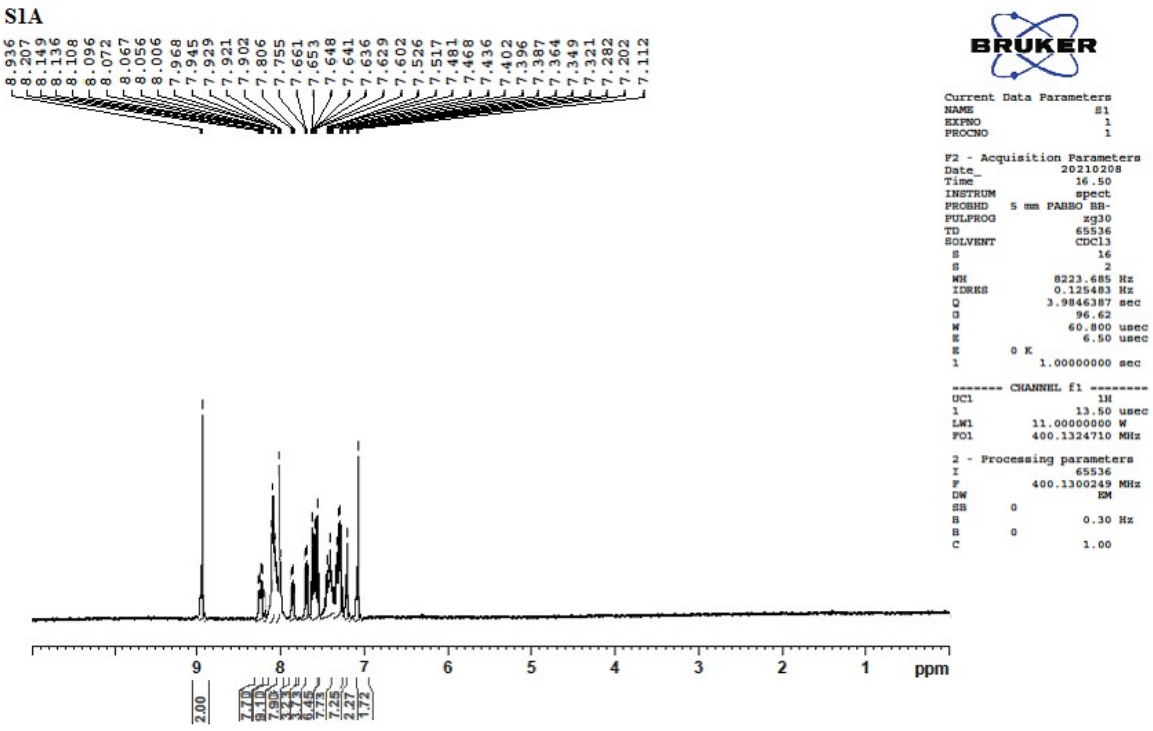

Plates S3. ^{1}H NMR spectrum of 4-(6,9-bis(4-(9H-carbazol-9-yl)phenyl)-2-(pyren-1-yl)-1H-phenanthro[9,10-d]imidazol-1-yl)naphthalene-1-carbonitrile (PPINCN-Cz).

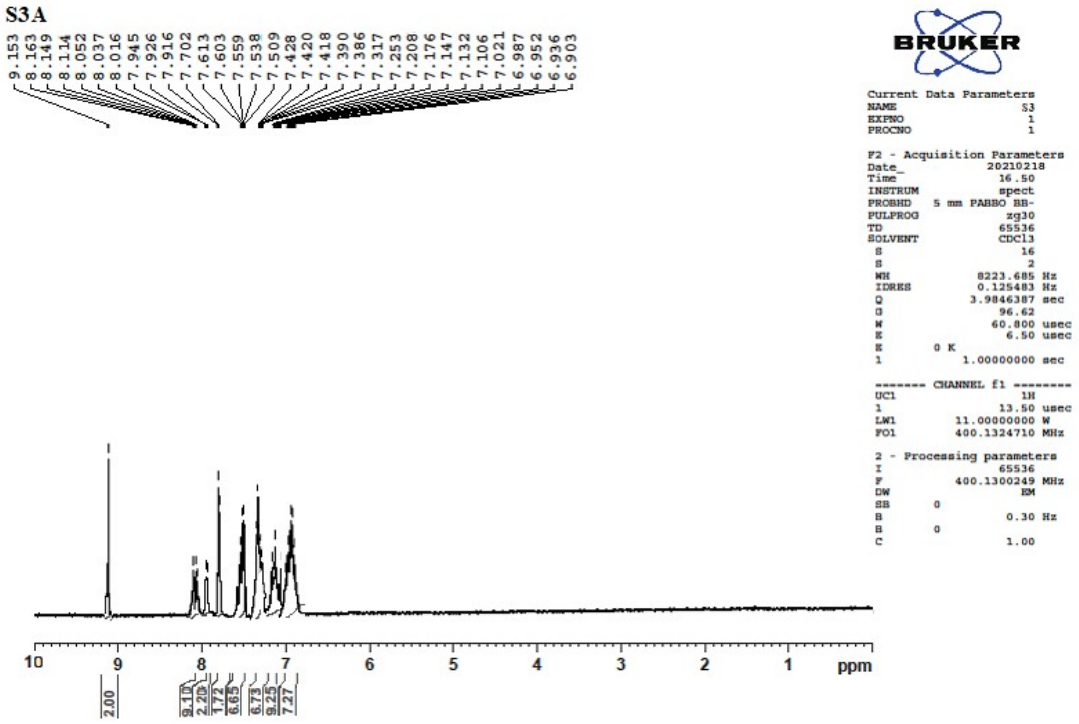

SI–II: Charge-Transfer intexes

The hole-particle pair interactions have been related to the distance covered during the excitations. One possible descript or Δr intex could be used to calculate the average distance which is weighted in function of the excitation coefficients.

$$\Delta r = \frac{\Sigma_{ia} k_{ia}^2 \left| \langle \varphi_a | r | \varphi_a \rangle - \langle \varphi_i | r | \varphi_i \rangle \right|}{\Sigma_{ia} K_{ia}^2} \quad \text{..... (S1)}$$

where, $\left| \langle \varphi_i | r | \varphi_i \rangle \right|$ is the norm of the orbital centroid [2–5]. Δr-intex will be expressed in Å. The density variation associated to the electronic transition is given by

$$\Delta\rho(r) = \rho_{EX}(r) - \rho_{GS}(r) \quad \text{..... (S2)}$$

where, $\rho_{GS}(r)$ and $\rho_{EX}(r)$ are the electronic densities of ground and excited states, respectively. Two functions, $\rho_+(r)$ and $\rho_-(r)$ corresponds to the points in space where an

increment or a depletion of the density upon absorption is produced and they can be defined as follows:

$$\rho_+(r) = \begin{Bmatrix} \Delta\rho(r) if \Delta\rho(r) > 0 \\ 0 \quad if \Delta\rho(r) < 0 \end{Bmatrix} \quad \text{..... (S3)}$$

$$\rho_-(r) = \begin{Bmatrix} \Delta\rho(r) if \Delta\rho(r) < 0 \\ 0 \quad if \Delta\rho(r) > 0 \end{Bmatrix} \quad \text{..... (S4)}$$

The barycenters of the spatial regions R_+ and R_- are related with $\rho_+(r)$ and $\rho_-(r)$ and are shown as,

$$R_+ = \frac{\int r\rho_+(r)dr}{\int \rho_+(r)dr} = (x_+, y_+, z_+) \quad \text{..... (S5)}$$

$$R_- = \frac{\int r\rho_-(r)dr}{\int \rho_-(r)dr} = (x_-, y_-, z_-) \quad \text{..... (S6)}$$

The spatial distance (D_{CT}) between the two barycenters R_+ and R_- of density distribution scan thus, be used to measure the CT excitation length

$$D_{CT} = |R_+ - R_-| \quad \text{..... (S7)}$$

The transferred charge (q_{CT}) can be obtained by integrating over all space $\rho_+(\rho_-)$,. Variation in dipole moment between the ground and the excited states (μ_{CT}) can be computed by the following relation:

$$\|\mu_{CT}\| = D_{CT}\int \rho_+(r)dr = D_{CT}\int \rho_-(r)dr \quad \text{..... (S8)}$$

$$= D_{CT}q_{CT} \quad \text{..... (S9)}$$

The difference between the dipole moments $\|\mu_{CT}\|$ have been computed for the ground and the excited states ($\Delta\mu_{ES\text{-}GS}$). The two centroids of charges (C^+/C^-) associated to the positive

and negative density regions are calculated as follows: First the root-mean-square deviations along the three axis (σ_{aj}, j = x, y, z; a = + or –) are computed as,

$$\sigma_{a,j} = \sqrt{\frac{\sum_i \rho_a(r_i)(j_i - j_a)^2}{\sum_i \rho_a(r_i)}} \quad \text{..... (S10)}$$

The two centroids (C_+ and C_-) are defined as,

$$C_+(r) = A_+ e\left(-\frac{(x - x_+)^2}{2\sigma_{+x}^2} - \frac{(y - y_+)^2}{2\sigma_{+y}^2} - \frac{(z - z_+)^2}{2\sigma_{+z}^2}\right) \quad \text{..... (S11)}$$

$$C_-(r) = A_- e\left(-\frac{(x - x_-)^2}{2\sigma_{-x}^2} - \frac{(y - y_-)^2}{2\sigma_{-y}^2} - \frac{(z - z_-)^2}{2\sigma_{-z}^2}\right) \quad \text{..... (S12)}$$

The normalization factors (A+ and A_) are used to impose the integrated charge on the centroid to be equal to the corresponding density change integrated in the whole space:

$$A_+ = \frac{\int \rho_+(r)dr}{\int e(-\frac{(x - x_-)^2}{2\sigma_{+x}^2} - \frac{(y - y_-)^2}{2\sigma_{+y}^2} - \frac{(z - z_-)^2}{2\sigma_{+z}^2})dr} \quad \text{..... (S13)}$$

$$A_- = \frac{\int \rho_-(r)dr}{\int e(-\frac{(x - x_-)^2}{2\sigma_{-x}^2} - \frac{(y - y_-)^2}{2\sigma_{-y}^2} - \frac{(z - z_-)^2}{2\sigma_{-z}^2})dr} \quad \text{..... (S14)}$$

H index is defined as half of the sum of the centroids axis along the D-A direction, if the D-A direction is along the X axis, H is defined by the relation:

$$H = \frac{\sigma_{+x} + \sigma_{-x}}{2} \quad \text{..... (S15)}$$

The centroid along X axis is expected. The t intex represents the difference between D_{CT} and H:

$$t = D_{CT} - H \quad \text{..... (S16)}$$

Figure S1. Natural transition orbital pairs (HONTOs and LUNTOs) with transition character for singlet states (S_1-S_5) and triplet states (T_1-T_5) of PPINCN [*f*-oscillator strength and % weights of hole-particle].

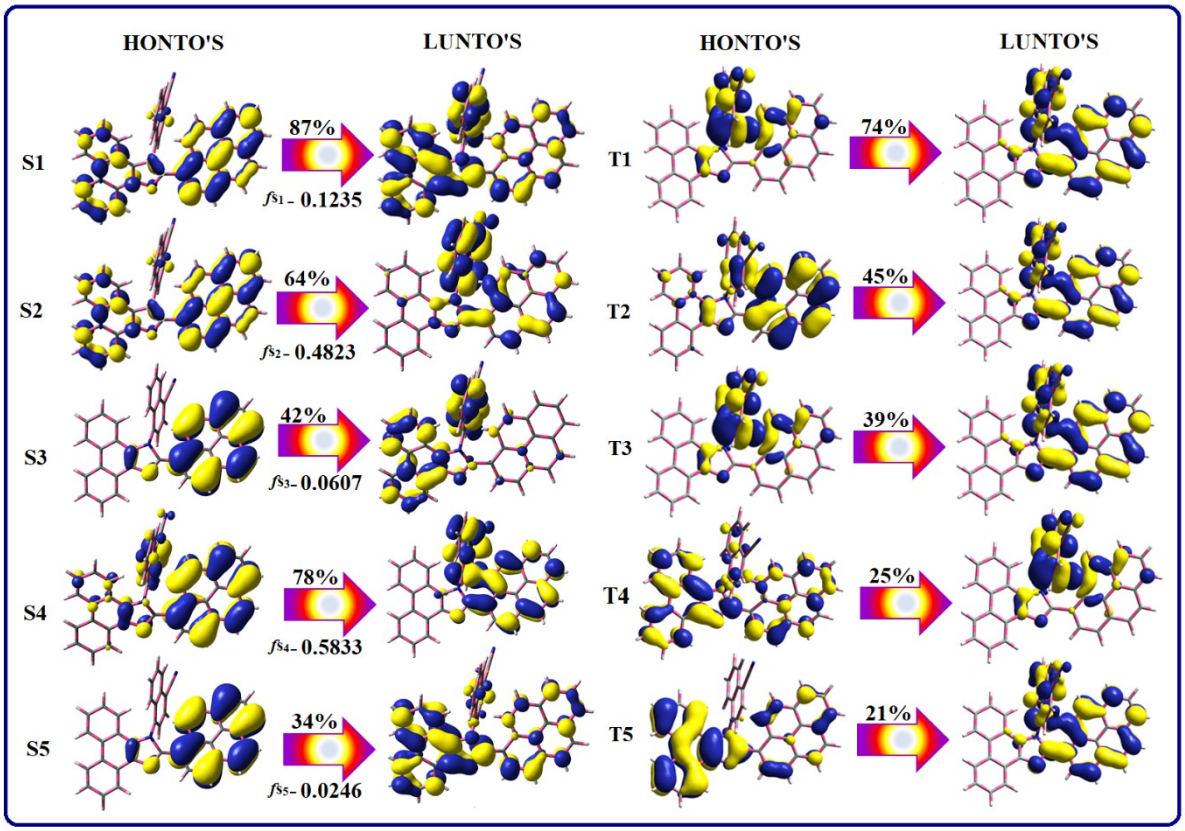

Figure S2. Natural transition orbital pairs (HONTOs and LUNTOs) with transition character for singlet states (S_1-S_5) and triplet states (T_1-T_5) of PPINCN-TPE [*f*-oscillator strength and % weights of hole-particle].

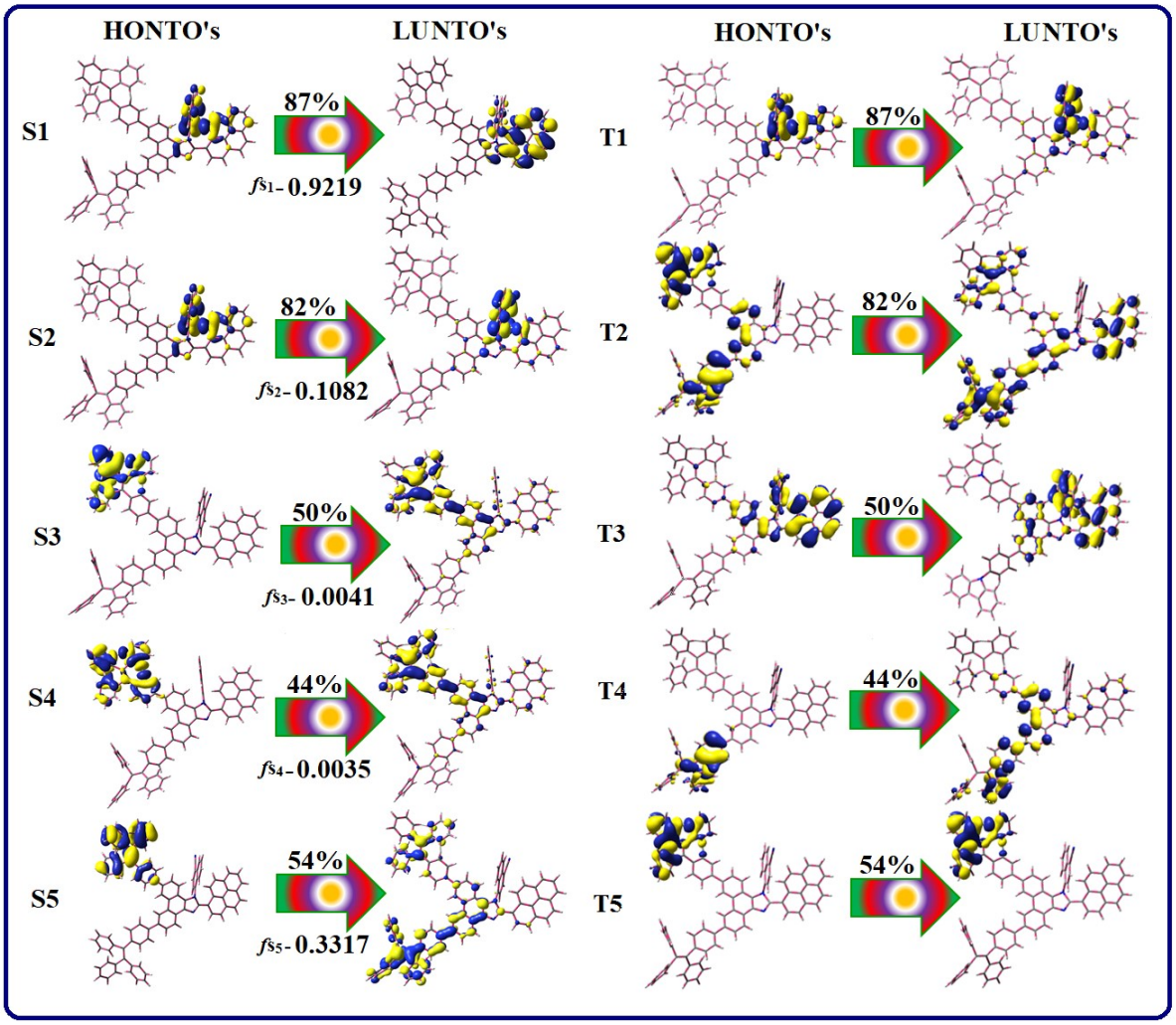

Figure S3. Emission spectra and UV illumination of (a) PPINCN; (b) PPINCN-TPE and (c) PPINCN-Cz in THF-H_2O mixture with different water fractions and (d) ML and PL spectra.

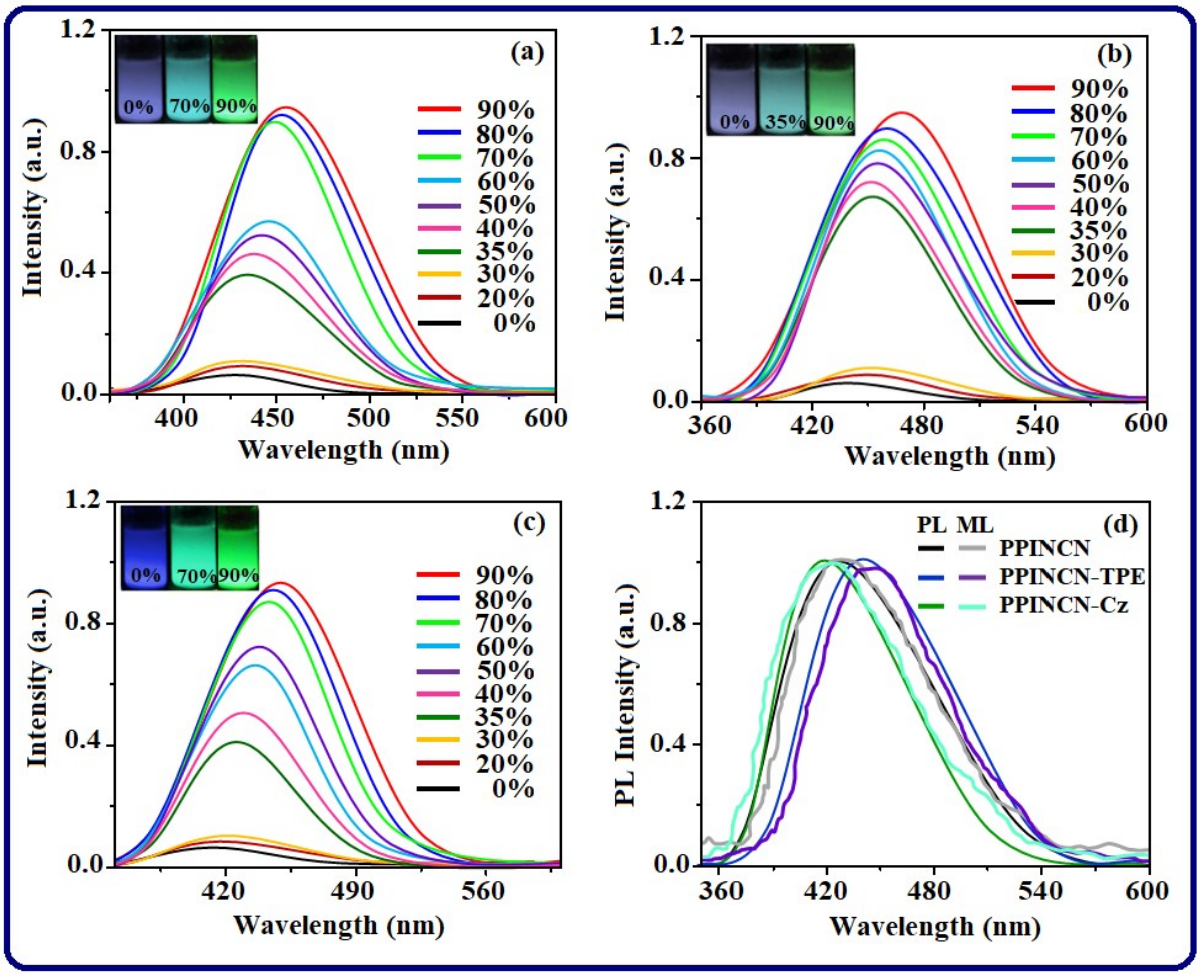

Figure S4. (a) Optimised geomentry with dihedral angles, HOMO-LUMO orbitals and net dipolemoment of couples I-III of PPINCN and (b) Intermolecular interactions of couples I-III of PPINCN.

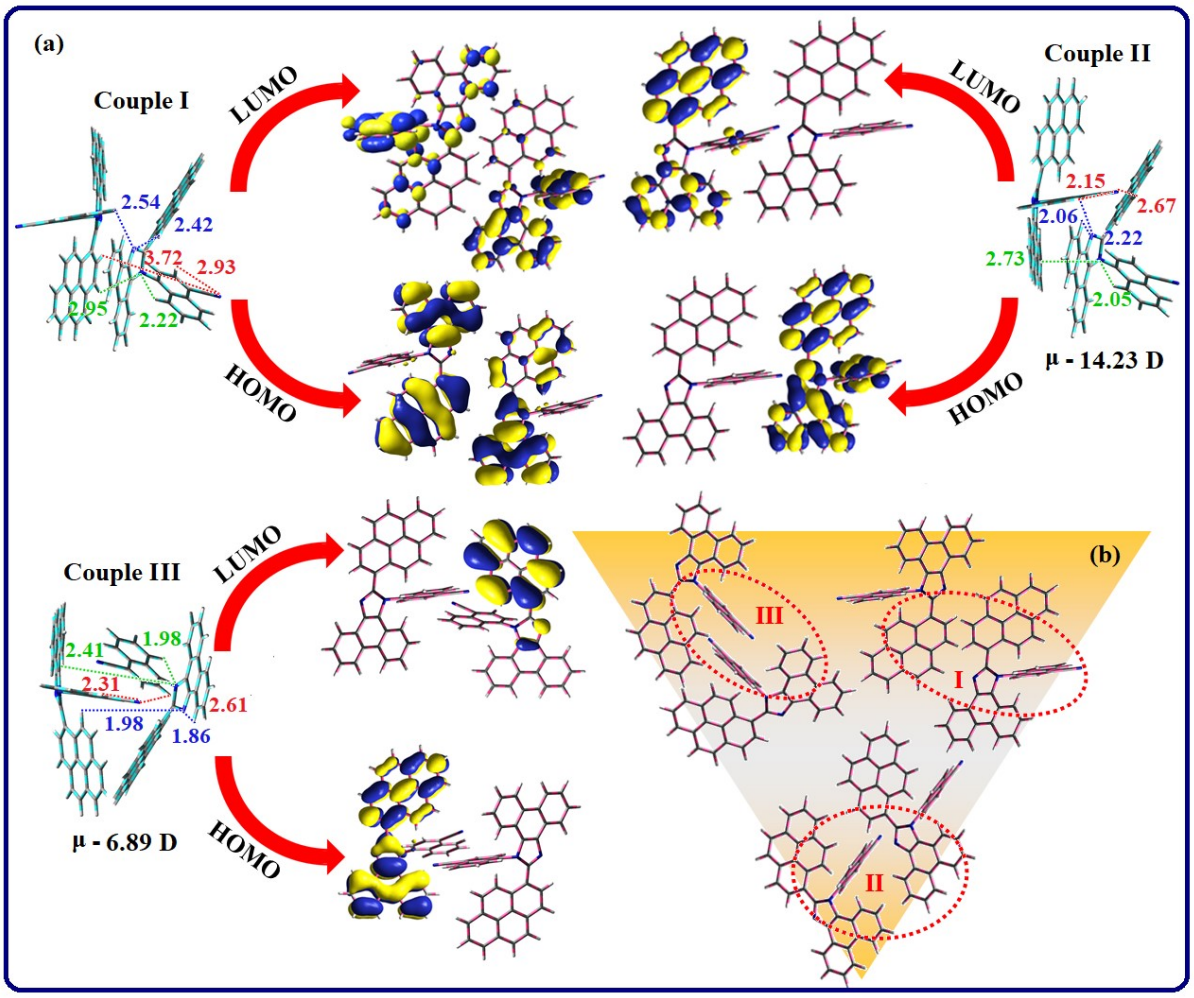

Figure S5. (a) Optimised geomentry with dihedral angles, HOMO-LUMO orbitals and net dipolemoment of couples I-III of PPINCN-TPE and (b) Intermolecular interactions of couples I-III of PPINCN-TPE.

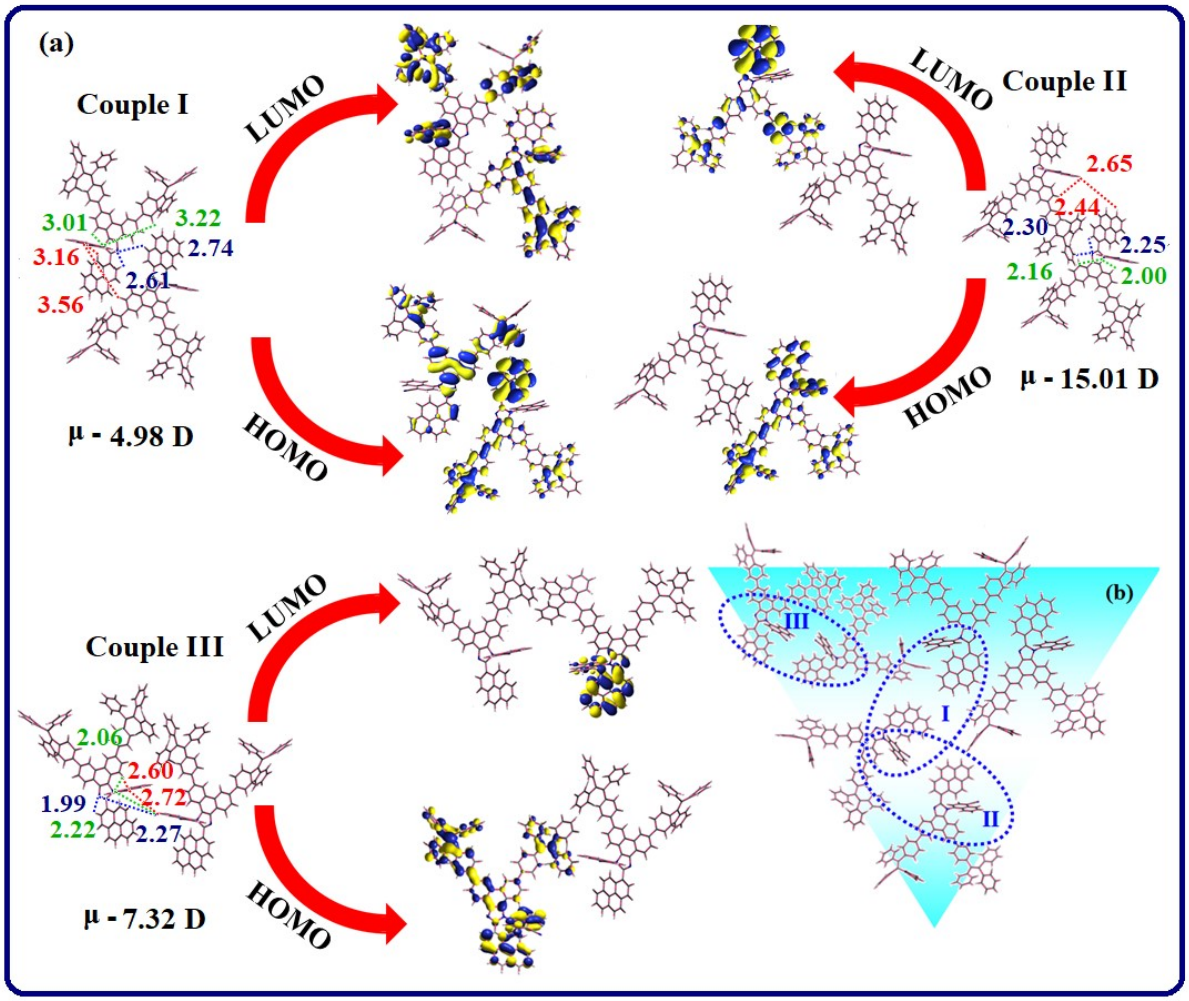

SI-III: (a) Solvatochromism for HLCT character

The solvatochromic effect using Lippert-Mataga plot has been displayed in Figure S6. As the solvent polarity increased the blue emitters exhibit a larger red shift which supports the charge transfer (CT). From Lippert-Mataga plot, the ground state dipolemoment (μ_g) can be calculated: $hc(\tilde{\upsilon}_{abs} - \tilde{\upsilon}_{flu}) = hc(hc\tilde{\upsilon}_{abs}^{vac} - hc\tilde{\upsilon}_{flu}^{vac}) + 2(\mu_e - \mu_g)^2 / a_o^3 [(\varepsilon - 1/ 2\varepsilon + 1) - ½ (n^2 - 1/ 2n^2 + 1)]$ [μ_g and μ_e - ground state and excited state dipolemoment, $\tilde{\upsilon}_{abs}$ and $\tilde{\upsilon}_{abs}^{vac}$ - solvent-equilibrated absorption maxima (λ_{abs}) and extrapolated to gas phase, $\tilde{\upsilon}_{flu}$ and $\tilde{\upsilon}_{flu}^{vac}$ - solvent equilibrated fluorescence maxima (λ_{emi}) and extrapolated to gas-phase, respectively, a_o - onsager cavity and ε and n solvent dielectric constant and refractive index, respectively]. The non-linear correlation of Stokes shift *vs* solvent polarity function reveal that transformation of fitted line between ethyl ether and methylene chloride: non-linear correlation supports the presence of both locally excited state (LE) and charge transfer excited state (CT). All these results show that CT dominates in more polar medium and LE dominates in low polar solvent and there is mixed contribution of LE and CT in medium polar solvents.

The optical characteristics of emissive materials were studied in solution as well as solid by absorption and emission studies. When cyano group is incorporated, the modification in charge-transfer state red-shifted the absorption and emission. The CN group rarely influences the electronic properties as well as band-gap. It is in accordance with quantum chemical calculations. The emission peak was red shifted as increasing the solvent polarity because of polarization induced optical shift (Figure S6). The PL spectra gradually widened indicates that their excited state have strong CT character when compared to ground state and further stabilized by polar solvents.

Figure S6. Solvatochromism: (a) absorption and (b) emission spectra of PPINCN, PPINCN-TPE and PPINCN-Cz.

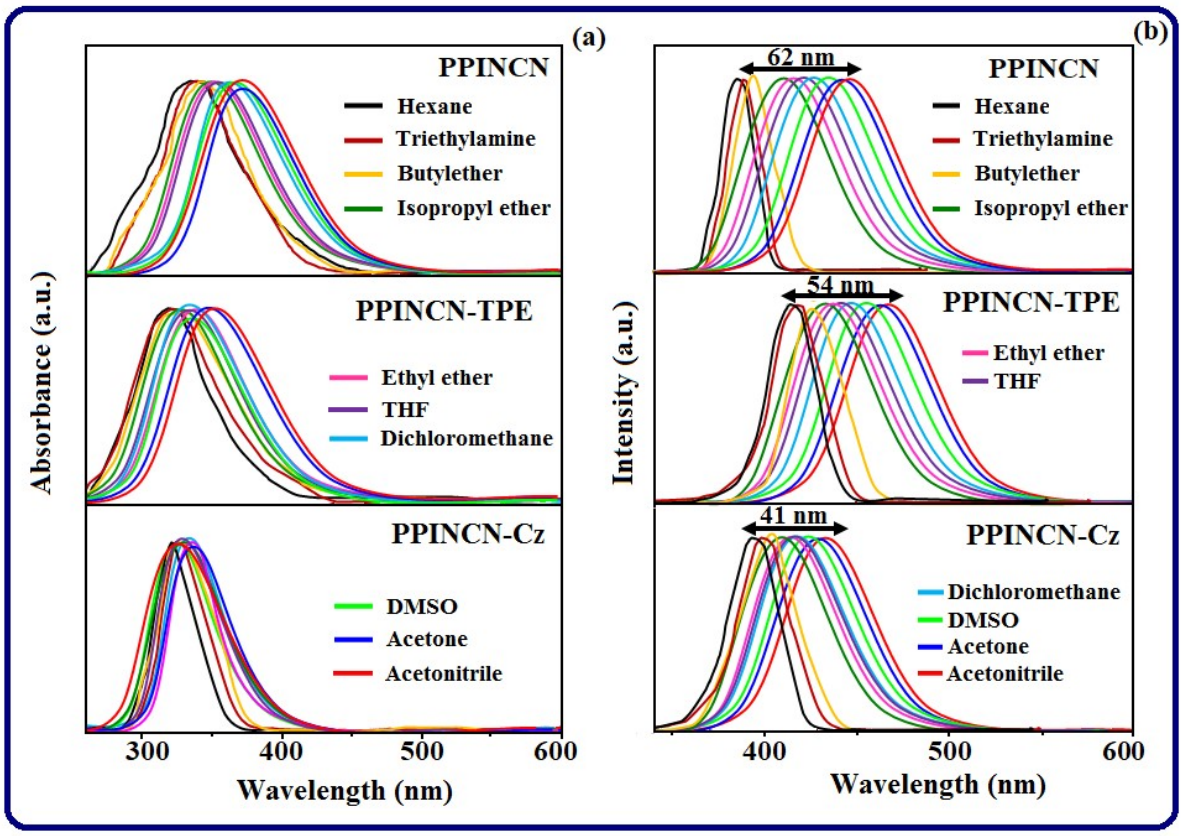

(b) Transition density matrix (TDM) plot

The existence of LE and CT states can be discussed from wave function of electron-hole pairs transition density matrix (TDM) plot. The diagonal region represents LE component and off-diagonal region shows CT component. Upon excitation, electron transferred from donor and localized on acceptor: depending upon intramolecular geometrical and electronic coupling, transferred electron delocalized from the region of nearby donor to the vicinity of acceptor. This effect can be qualitatively studied by analyzing electron density distribution at ground and excited states. Computed electron-hole properties, distance between hole and electron, transition density, H and t indexes and RMSD of electron and hole of these emitters are displayed in Tables S10-S12.

The integral value of hole and electron with transition density have been shown in Tables S7 - S9. The integral overlap of hole-electron distribution (S) is a measure of spatial separation of hole and electron. The integral overlap (S) of hole and electron and distance (D) between centroids of hole and electron proved the existence of LE and CT states. These emitters show small S and high D, indicates higher charge transfer (CT) variation of dipolemoment with respect to S_0 state. These values are directly evaluated based on the position of centroid of hole and electron. RMSD of hole or electron characterizes their distribution breadth: RMSD of both electron and hole is higher in X direction indicates electron and hole distribution is much broader in Y and Z directions (Tables S10-S12). The overlap between the region of density depletion and increment have been visualised by using two centroids of charges (equations S9 and S10). The H and t indexes for PPINCN, PPINCN-TPE and PPINCN-Cz are tabulated (Tables S10-S12).The CT intex, *i.e.* index difference between D_{CT} and H index is another measure of the separation of hole-electron (equations S15 and S16). The D_{CT} of PPINCN, PPINCN-TPE and PPINCN-Cz has been calculated to be 0.054/4.677/0.125, respectively and the calculated *H*/*t* indexes are of PPINCN (4.402/4.355),

PPINCN-TPE (4.885/2.199) and PPINCN-Cz (6.990/6.882) (Figure S12 and Table S13). For PPINCN, PPINCN-TPE and PPINCN-Cz, the non-zero *t* is negative in all directions: overlap of hole and electron is very severe and eign value is greater than 0.96, supports the hybridization and described in terms of dominant excitation pair in terms of 94 % of transition.

The hybridization of these materials have been further evidenced by Δr intex (Tables S4 & S6). The Δr intex (equation S1) is average of hole (h^+)-electron (e^-) distance ($d_{h^+ - e^-}$) upon excitation which indicates the nature of excitation type, LE or CT: valence excitation (LE) is related to short distances ($d_{h^+ - e^-}$) while larger distances ($d_{h^+ - e^-}$) related to CT excitation. The triplet exciton is transformed to singlet exciton *via* RISC process with high energy excited state (hot CT channel) which are beneficial for triplet exciton conversion in electroluminescence process without delayed fluorescence [6, 7]. The CT excitons have been formed with weak binding energy (E_b) on higher excited states [8, 9]. As a result, the exciton utilization can be harvested in PPINCN, PPINCN-TPE and PPINCN-Cz like phosphorescent materials. The hybridization between LE and CT components leads to high EUE and enhanced OLEDs performances (Table 3) [9].

Figure S7. Contour plot of transition density matrices (TDM) with hole and particle distribution [green - increasing electron density and blue- decreasing electron density] of PPINCN [S_1-S_3 states: density = transition = n /IOp(6/8=3)].

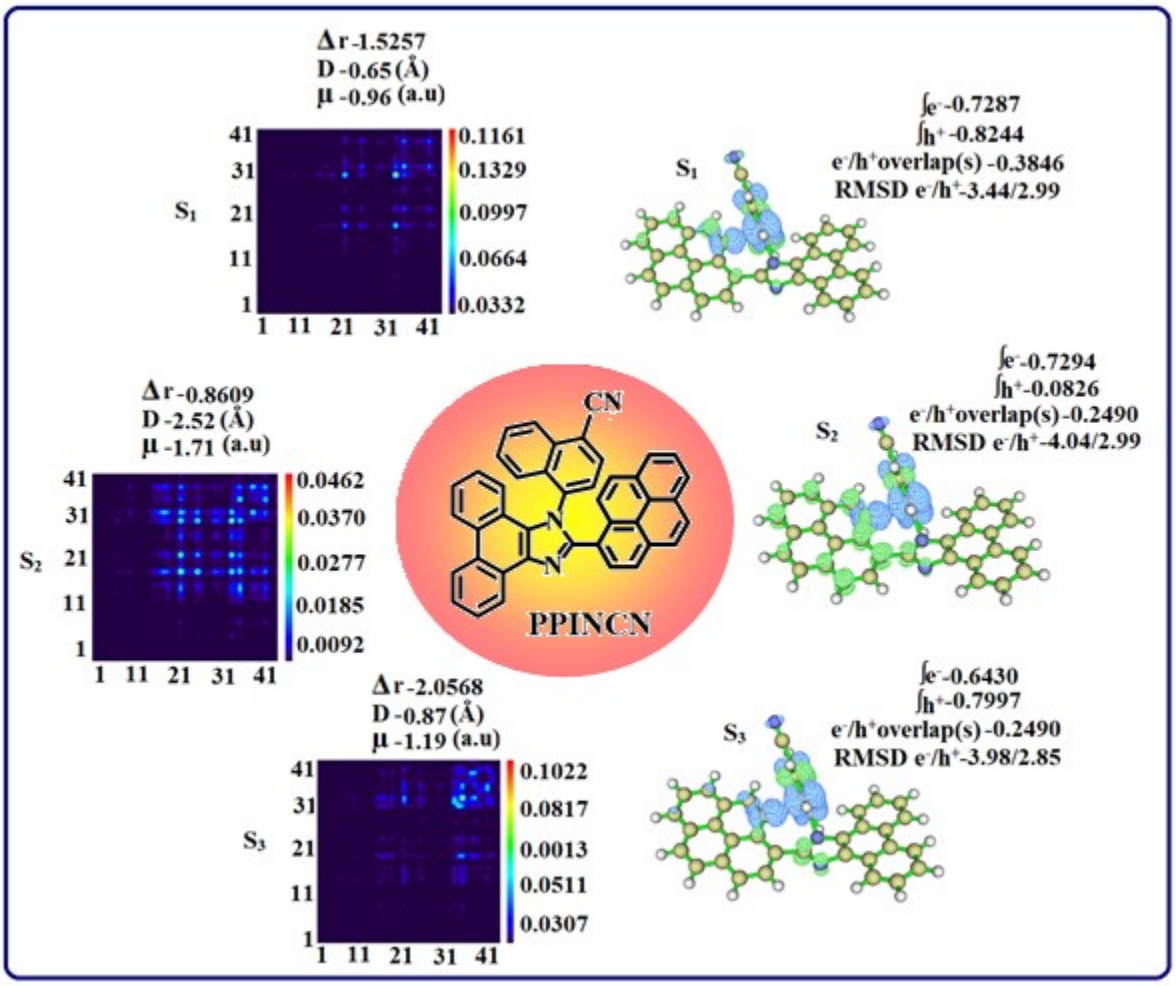

Figure S8. Contour plot of transition density matrices (TDM) and hole and particle distribution [green - increasing electron density and blue- decreasing electron density] of PPINCN-TPE [S_1-S_3 states: density = transition = n /IOp(6/8=3)].

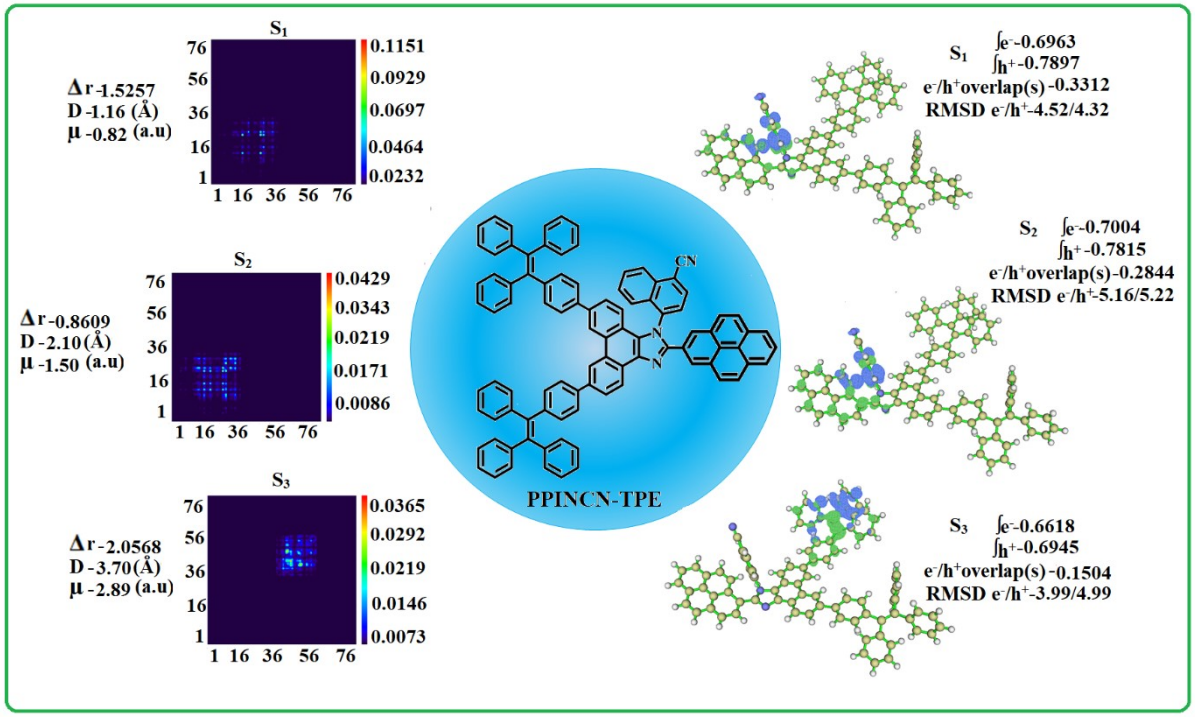

Figure S9. Contour plot of transition density matrices (TDM) and hole and particle distribution [green - increasing electron density and blue- decreasing electron density] of PPINCN-Cz [S_1-S_3 states: density = transition = n /IOp(6/8=3)].

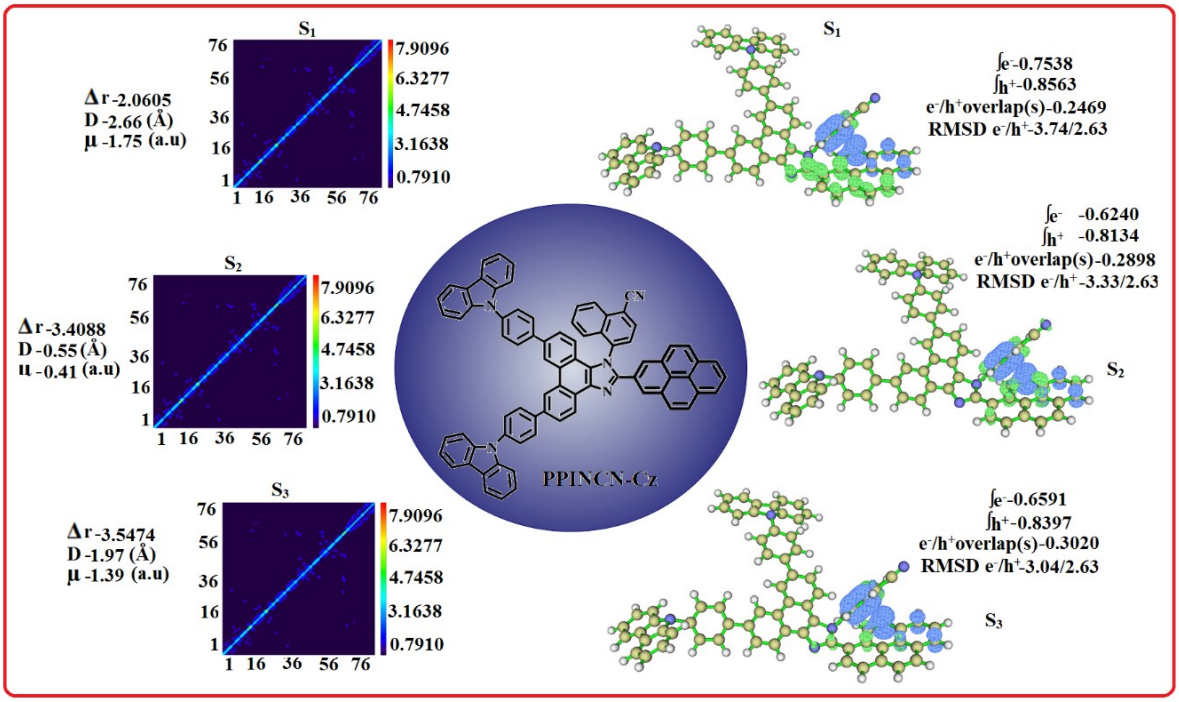

(c) Hot exciton mechanism

The interstate hybridization coupling between LE and CT state wave function are of $\Psi_{S_1/S_2} = c_{LE}.\Psi_{LE} \pm c_{CT}.\Psi_{CT}$. The % CT of these emitters increases as increasing the aromatic fragment size and also partially influenced by steric hindrance. The % LE in S1 state, these emitter's exhibit higher photoluminance efficiency (η_{PL}) and high lying CT state increased the EUE (Figure 9). Therefore, degree of hybridization between LE and CT states depends not only initial E_{LE}-E_{CT} energy gap but also their interstate coupling strength [10]. Especially, the large energy differences of the initial LE and CT states in PPINCN and PPINCN-TPE lead to non-equivalent hybridization between LE and CT states, whereas the isoenergetic LE and CT states of PPINCN-TPE belongs to quasi-equivalent hybridization. The vertical excitation energies for the pure LE state were obtained for the corresponding conjugated molecular backbone by replacing the cyano group with hydrogen atoms and the

vertical excitation energy of pure CT state were roughly estimated according to the energy conservation ($E_{S1} + E_{S2} = E_{LE} + E_{CT}$).

In hot exciton mechanism, the core concept is increasing the rate of h_{RISC} (k_{hRISC}) from Tn ($n \geq 2$) to Sm ($m \geq 1$), while decreasing the rate of internal conversion (k_{IC}) from Tn ($n \geq 2$) to T1. When $k_{hRISC} \gg k_{IC}$, the non-radiative triplet excitons could be fully converted into radiative singlet excitons, resulting in improvement of device efficiency. According to Fermi's golden rule [5], k_{hRISC} depends on ΔE_{ST} and spin-orbit coupling (SOC), as expressed in formula S17

$$k_{hRISC} \propto \left| \frac{\left\langle \Psi_{S_m} \middle| \hat{H}_{SO} \middle| \Psi_{T_n} \right\rangle}{\Delta E_{S_m T_n}} \right|^2 \quad (m \geq 1, n \geq 2) \text{.....S17}$$

in which $\Psi_{T_n}$and Ψ_{S_m}represent the wave functions of initial (Tn, $n \geq 2$) and final (Sm, $m \geq 1$) states of h_{RISC}, respectively, SO is the operator for SOC $\left\langle \Psi_{S_m} \middle| \hat{H}_{SO} \middle| \Psi_{T_n} \right\rangle$ and represent the SOC matrix element and the energy difference between Tn and Sm, $\Delta E_{S_m T_n}$. Therefore, increasing k_{hRISC} from T_n to S_m requires small $\Delta E_{S_m T_n}$and large SOC. On the other hand, k_{IC} can be expressed by using the following formula S18 [6]

$$k_{IC} \propto \left| \frac{\left\langle \Psi_{T_n} \middle| \hat{T}_N \middle| \Psi_{T_1} \right\rangle}{\Delta E_{T_n T_1}} \right|^2 (n \geq 2) \quad \text{.....S18}$$

where, $\Psi_{T_n}$and Ψ_{T_1}represent the wave functions of high-lying (Tn, $n \geq 2$) and low-lying triplet states of IC process, respectively, $\Psi_{T_n}$and Ψ_{T_1}, $\Psi_{T_n}\left\langle \hat{T}_N \middle| \Psi_{T_1} \right\rangle \Delta E_{T_n T_1}$ is the electronic operator describing the oupling energy gap between Tn and T1 states. In consequence, decreasing k_{IC} from Tn to T1 requires poor electronic coupling factor and large $\Delta E_{T_n T_1}$.

Usually, a large energy gap between the initial and final state plays a critical role in the slow k_{IC}. So, three positive factors including large $\Delta E_{T_nT_1}$, small $\Delta E_{S_mT_1}$ and large $\left\langle \Psi_{S_m} \middle| \hat{T}_{S_0} \middle| \Psi_{T_n} \right\rangle$ are liable to achieve efficient OLEDs with "hot exciton" mechanism.

Figure S10. (a) Current density-electric field intensity curve of single carrier devices and Energy level diagram of (b) Non-doped; (c) Doped devices and (d) Doped devices with 2CNQTPA.

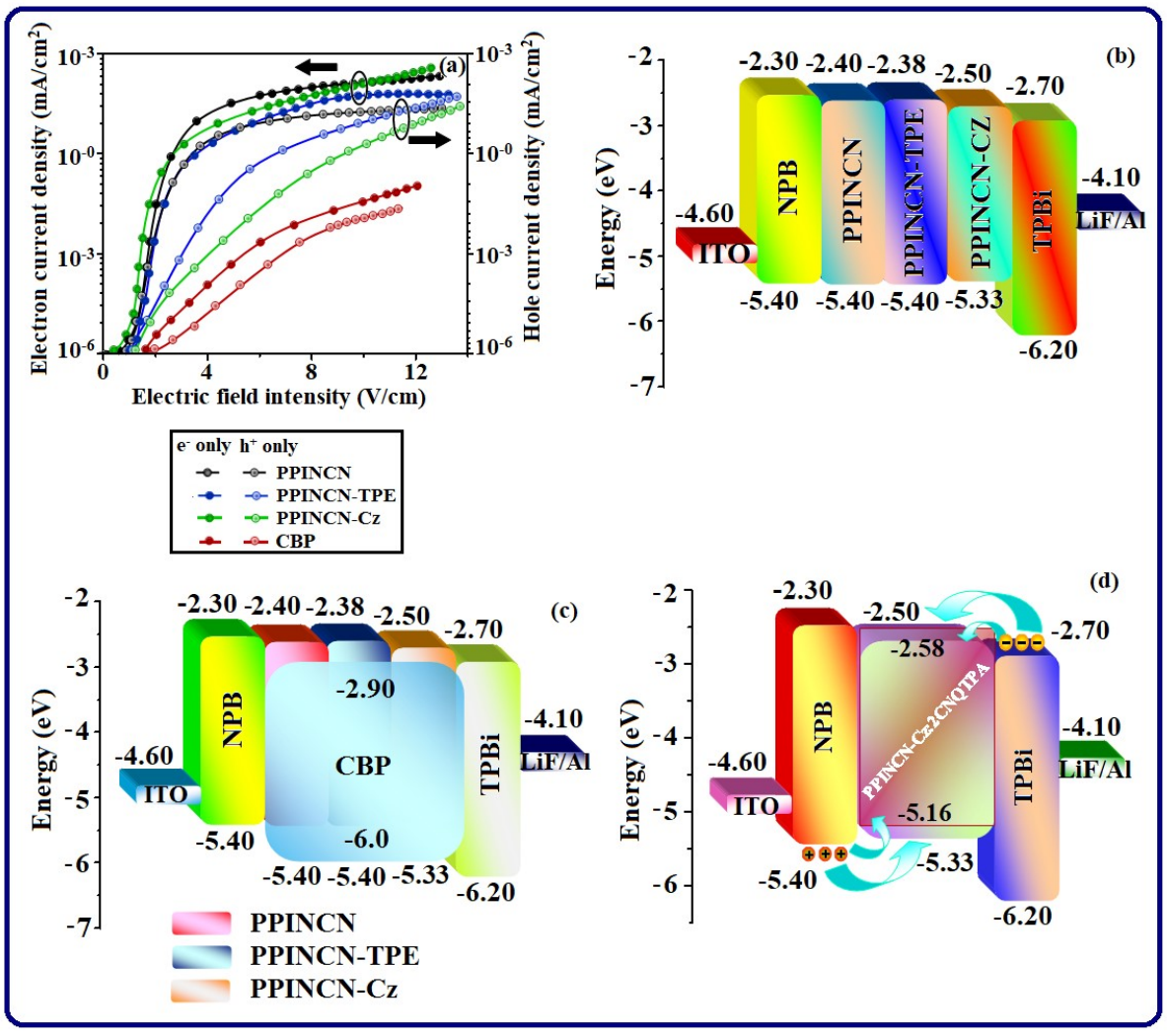

Figure S11. PL spectra of emissive materials in different voltages.

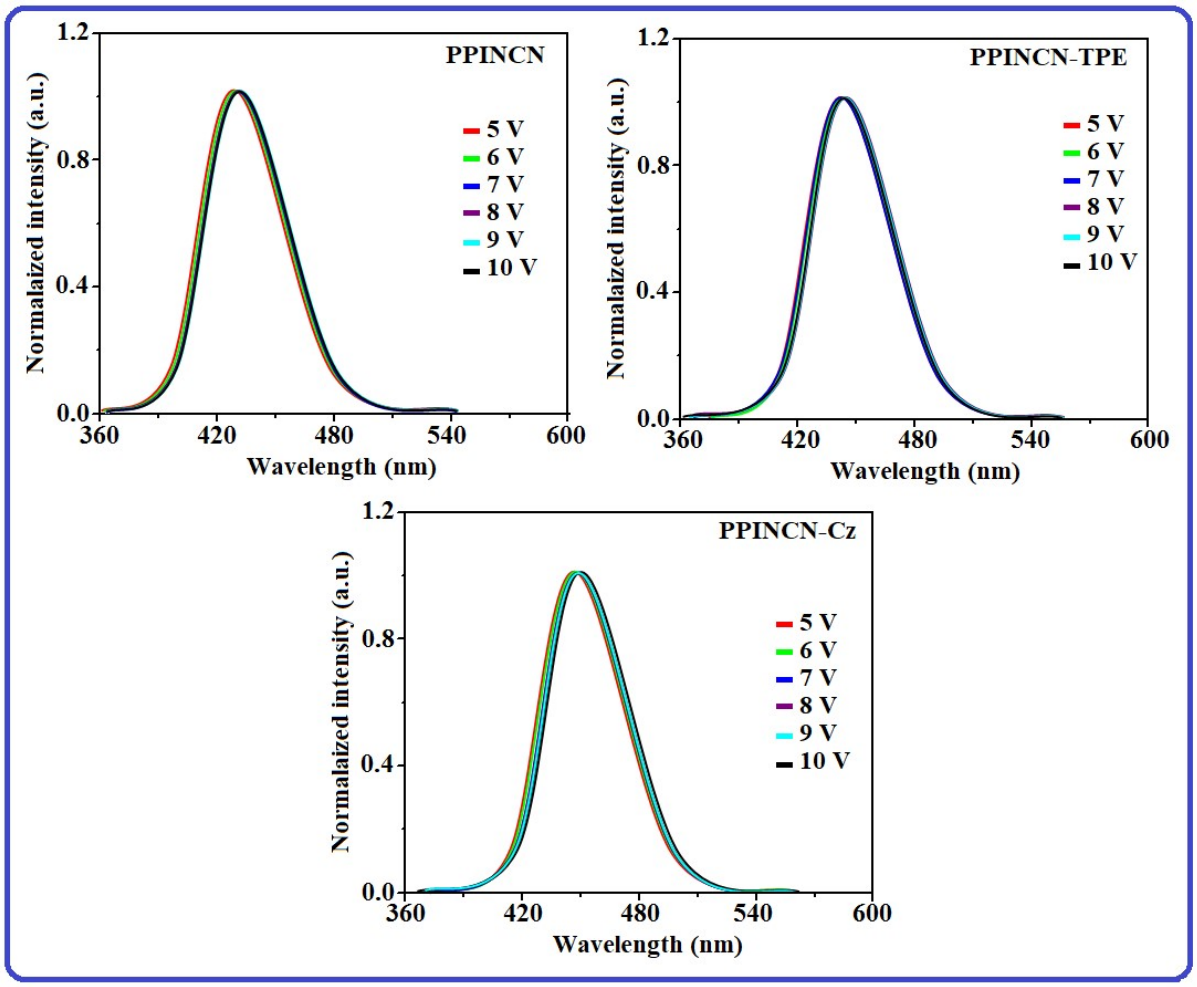

Figure S12. (a) Current-density-luminance curves of device PPINCN, PPINCN-TPE and PPINCN-Cz and (b) Transient decay spectra of PPINCN, PPINCN-TPE and PPINCN-Cz in neat films.

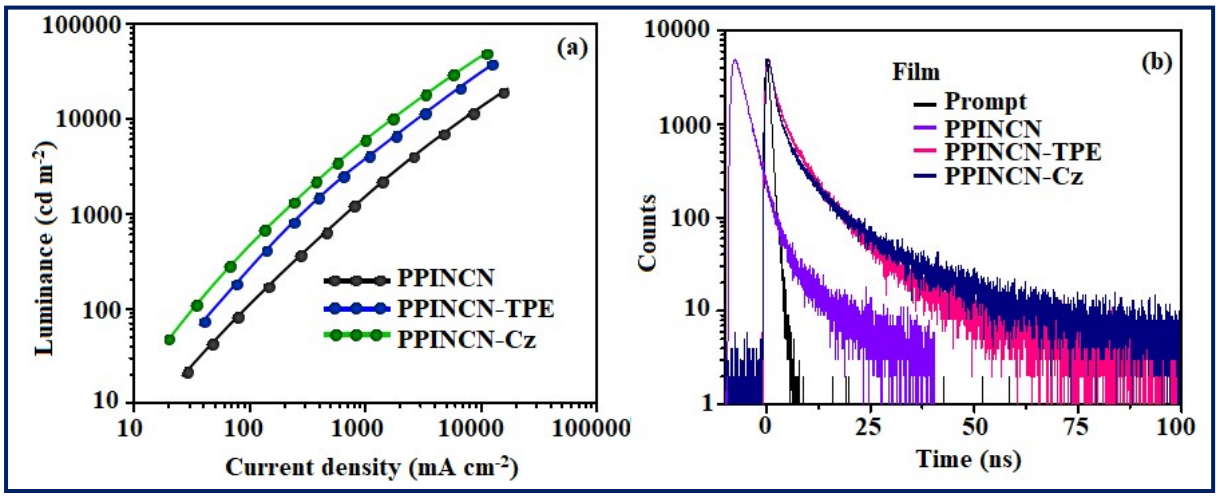

Figure S13. Graphical representation of D_{CT} and centroid of charges [C+(r) / C-(r); iso surface for PPINCN, PPINCN-TPE and PPINCN-Cz (0.1 a.u)].

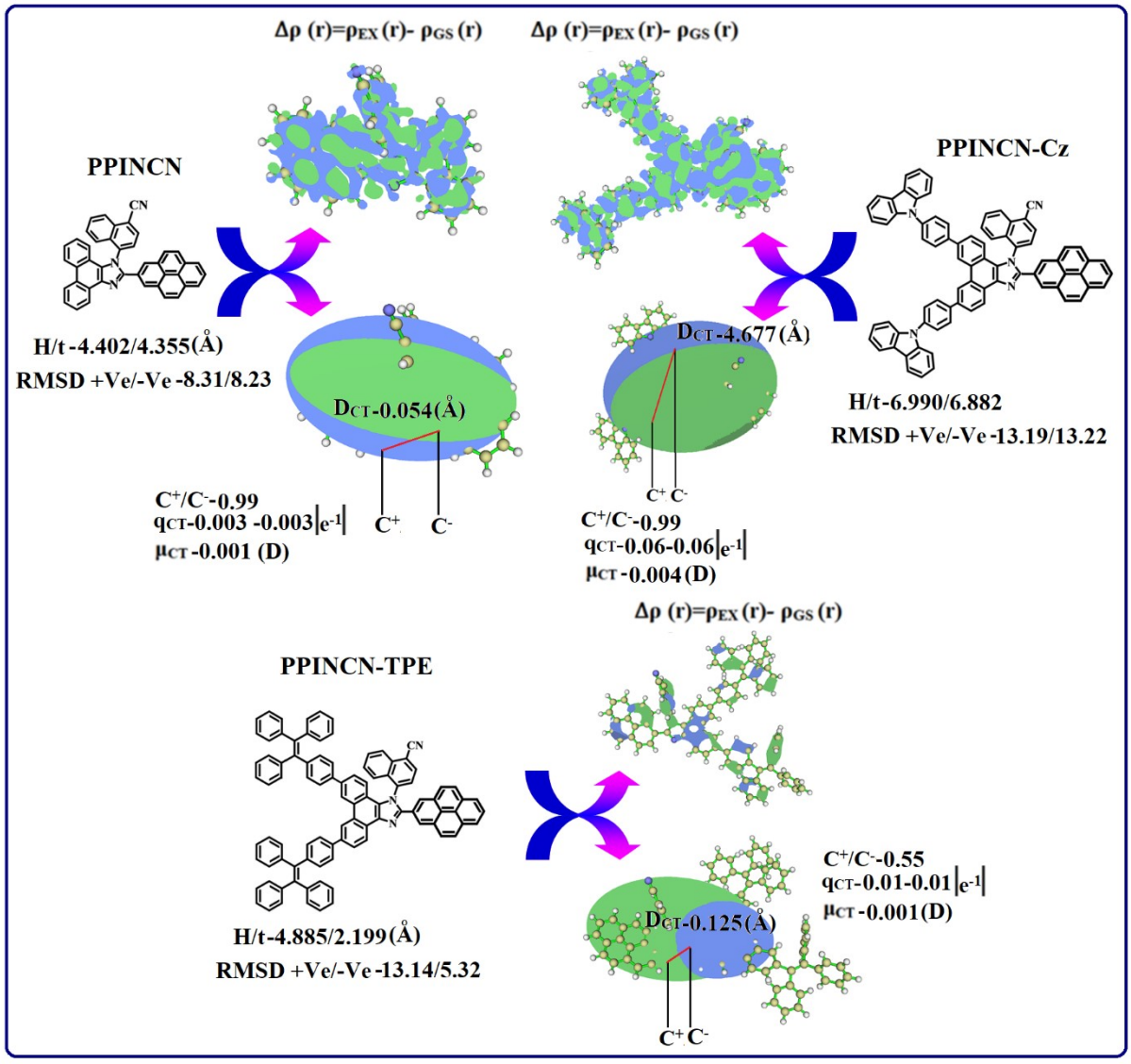

SI-IV: Potential energy scan (PES)

The potential energy surface (PES) scan have been plotted as a function of twist angle between C2 substituent and phenanthroimidazole core in gas phase and different polar solvents (Figures S14 – S17). In gas phase, it is impossible for S3 mixing with S1 state as a result of large energy gap between them. An increasing solvent polarity, the large dipole moment of S3 state leads to energetic stabilization. In low polarity solvent (hexane), S3 state can intercross with S1 state whereas in high polarity solvent (acetonitrile), S3 state energy decreases sharply and becomes lowest excited state. In moderate polar solvents (chloroform), the energetic closeness results in an enhanced mixing of S3 with S1. Therefore, S1 state is dominated by LE character in low polar medium; S1 state is dominated by mixing LE and CT character in moderate polar medium and S1 state is dominated by CT character in high polar medium.

Figure S14. Potential energy surface scan (PES) diagram.

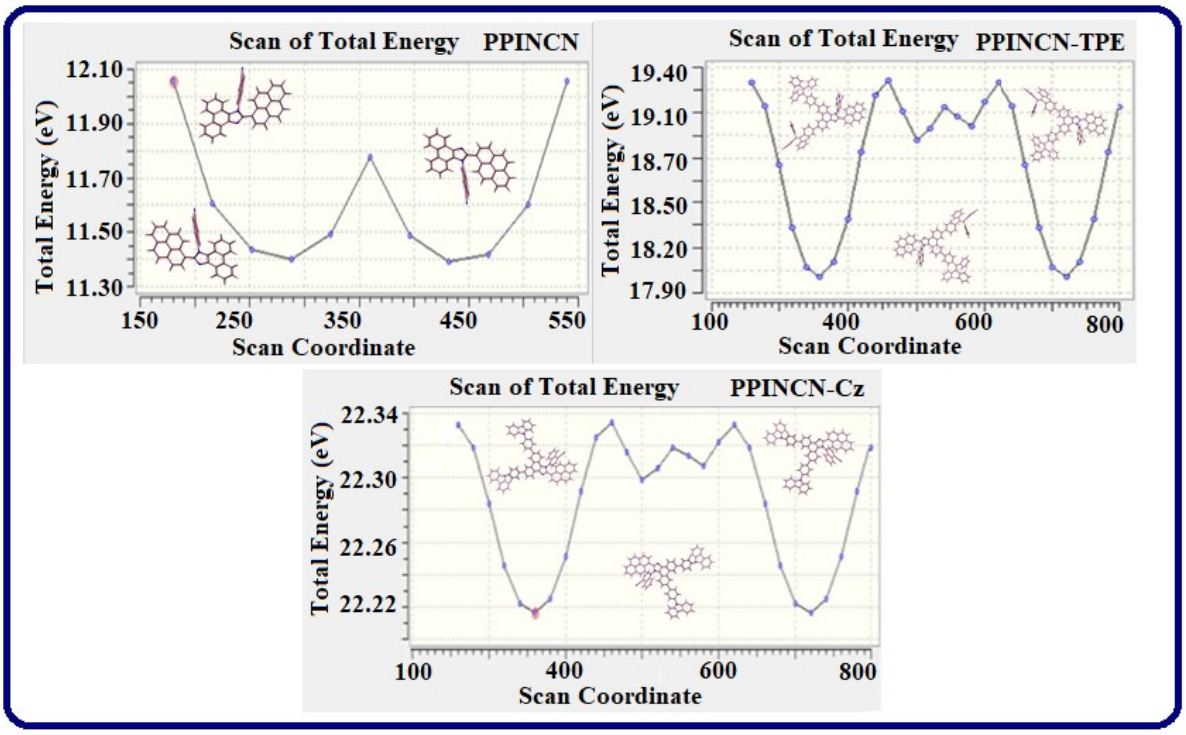

Figure S15. Potential energy scan (PES) of S_1-S_3 excited states of PPINCN with increasing solvent polarity.

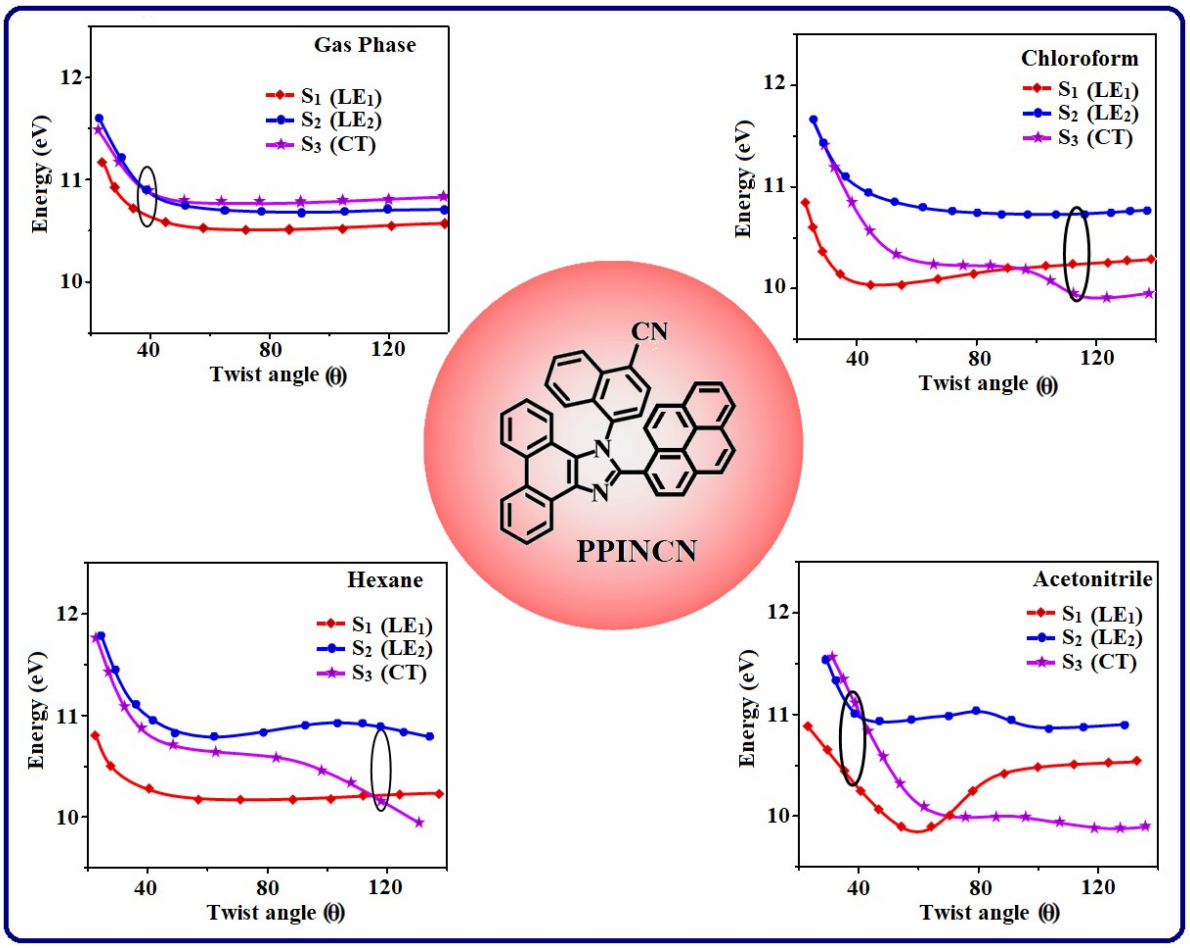

Figure S16. Potential energy scan (PES) of S_1-S_3 excited states of PPINCN-TPE with increasing solvent polarity.

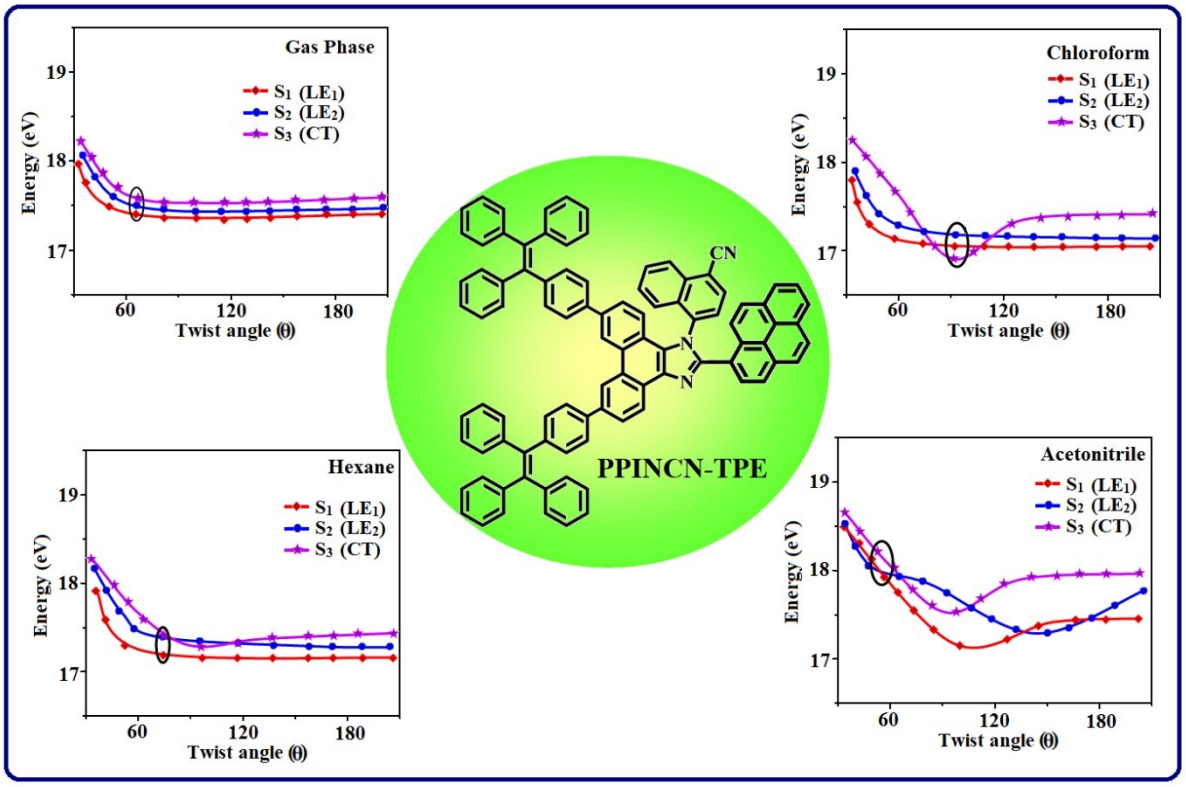

Figure S17. Potential energy scan (PES) of S_1-S_3 excited states of PPINCN-Cz with increasing solvent polarity.

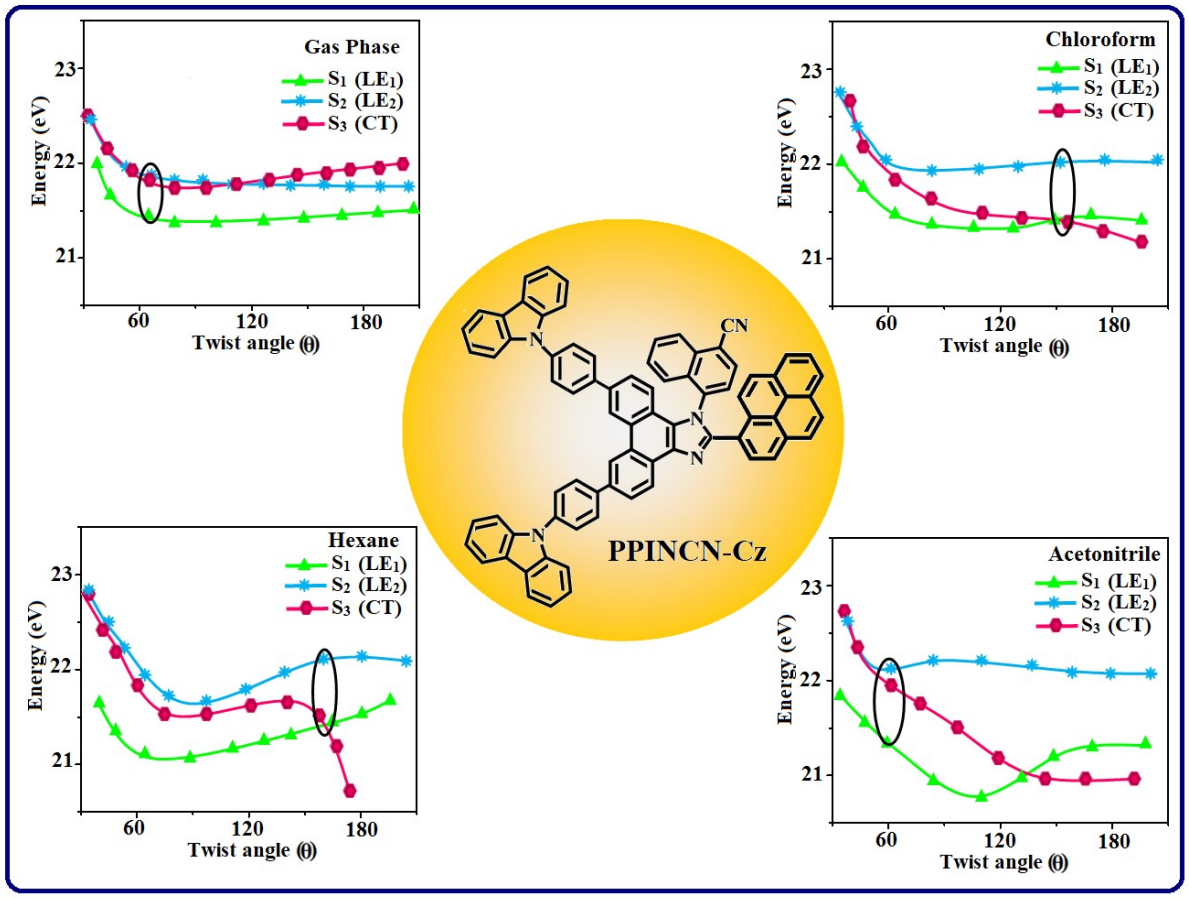

SI–V: Tables

Table S1. Computed excitation energy (eV), excitation coefficient, Δr intex (Å) oscillator strength (f) and dipolemoment (μ) for singlet and triplet states of PPINCN.

State	Excitation energy	Excitation coefficient	Δr intex	Oscillator strength (f)	μ (D)	NTO Transitions
S1	1.72	0.4471	1.5257	0.1235	0.96	$103 \xrightarrow{87\%} 104$
S2	2.17	0.4466	0.8609	0.4823	2.52	$103 \xrightarrow{64\%} 105$
S3	2.56	0.4287	2.0568	0.0607	1.19	$103 \xrightarrow{42\%} 107$
S4	2.87	0.4205	1.3484	0.5833	0.55	$102 \xrightarrow{78\%} 104$
S5	3.05	0.4014	2.0599	0.2426	1.50	$103 \xrightarrow{34\%} 106$
T1	0.28	0.4296	1.1438	0.0000	0.80	$103 \xrightarrow{74\%} 105$
T2	0.98	0.3644	1.6052	0.0000	0.61	$102 \xrightarrow{45\%} 104$
T3	1.57	0.3742	1.8698	0.0000	1.06	$103 \xrightarrow{39\%} 107$
T4	1.66	0.3689	2.8575	0.0000	0.33	$101 \xrightarrow{25\%} 106$
T5	1.85	0.3579	1.7925	0.0000	1.56	$103 \xrightarrow{21\%} 104$

Table S2. Computed excitation energy (eV), excitation coefficient, Δr intex (Å), oscillator strength (f) and dipolemoment (μ) for singlet and triplet states of PPINCN-TPE.

State	Excitation energy	Excitation coefficient	Δr intex	Oscillator strength (f)	μ (D)	NTO Transitions
S1	1.75	0.4571	1.5257	0.9219	1.16	$223 \xrightarrow{87\%} 226$
S2	2.27	0.4566	0.8609	0.1082	2.10	$223 \xrightarrow{82\%} 227$
S3	2.66	0.4487	2.0568	0.0041	3.70	$224 \xrightarrow{50\%} 228$
S4	2.97	0.4305	1.3484	0.0035	2.15	$222 \xrightarrow{44\%} 228$
S5	3.15	0.4114	2.0599	0.3317	1.56	$225 \xrightarrow{54\%} 229$
T1	1.53	0.4322	1.1349	0.0000	1.16	$223 \xrightarrow{65\%} 227$
T2	1.77	0.4277	1.6053	0.0000	2.10	$225 \xrightarrow{21\%} 229$
T3	2.03	0.4045	1.8698	0.0000	3.70	$221 \xrightarrow{47\%} 226$
T4	2.32	0.3787	2.8576	0.0000	2.15	$225 \xrightarrow{28\%} 234$
T5	2.34	0.4201	1.7925	0.0000	1.56	$224 \xrightarrow{24\%} 242$

Table S3. Computed excitation energy (eV), excitation coefficient, Δr intex (Å), oscillator strength (f) and dipolemoment (μ) for singlet and triplet states of PPINCN-Cz.

State	Excitation energy	Excitation coefficient	Δr intex	Oscillator strength (f)	μ (D)	NTO Transitions
S1	1.63	0.4635	2.0605	0.7103	2.66	$191 \xrightarrow{86\%} 192$
S2	1.69	0.4403	3.4088	0.6892	0.55	$189 \xrightarrow{74\%} 195$
S3	1.98	0.4546	3.5474	0.0737	1.97	$188 \xrightarrow{49\%} 194$
S4	2.49	0.4309	2.7546	0.1371	2.76	$191 \xrightarrow{69\%} 197$
S5	2.64	0.4282	3.3994	0.0537	3.45	$191 \xrightarrow{49\%} 201$
T1	0.33	0.4229	3.2301	0.0000	0.54	$191 \xrightarrow{76\%} 192$
T2	0.96	0.3738	3.3564	0.0000	1.82	$187 \xrightarrow{30\%} 195$
T3	1.30	0.3178	2.3511	0.0000	0.13	$190 \xrightarrow{22\%} 192$
T4	1.39	0.2615	2.4407	0.0000	0.13	$191 \xrightarrow{28\%} 192$
T5	1.63	0.2754	1.5980	0.0000	0.66	$188 \xrightarrow{19\%} 198$

Table S4. Photophysical properties of PPINCN in different solvents.

Solvents	ε	n	f (ε,n)	λ_{ab} (nm)	ν_{ab} (cm^{-1})	λ_{flu} (nm)	ν_{flu} (cm^{-1})	ν_{ss} (cm^{-1})	Φ_{PL}
Hexane	1.88	1.37	0.0004	332	30120.5	388	25773.2	4347.3	28.3
Triethylamine	2.42	1.401	0.048	333	30030.1	392	25510.2	4519.8	25.6
Butylether	3.08	1.399	0.096	336	29761.9	400	25000	4761.9	24.2
Isopropylether	3.88	1.368	0.145	343	29154.5	415	24096.4	5058.1	23.6
Ethyl ether	4.34	1.352	0.167	346	28901.7	419	23866.3	5035.4	21.0
THF	7.52	1.405	0.2096	348	28735.6	426	23474.2	5261.4	20
Dichloromethane	9.08	1.424	0.2183	352	28409.1	432	23148.1	5260.9	15.6
DMSO	47	1.478	0.2183	354	28248.6	440	22727.3	5521.3	11.4
Acetone	21.01	1.358	0.2847	358	27932.9	448	22321.4	5611.5	7.6
Acetonitrile	37.5	1.344	0.3053	358	27932.9	450	22222.2	5710.7	5.3

Table S5. Photophysical properties of PPINCN-TPE in different solvents.

Solvents	ε	n	f (ε,n)	λ_{ab} (nm)	ν_{ab} (cm^{-1})	λ_{flu} (nm)	ν_{flu} (cm^{-1})	ν_{ss} (cm^{-1})	Φ_{PL}
Hexane	1.88	1.37	0.0004	318	31446.5	415	24096.4	7350.1	69.8
Triethylamine	2.42	1.401	0.048	319	31347.9	418	23923.4	7424.5	60.6
Butylether	3.08	1.399	0.096	322	31055.9	426	23474.2	7581.7	52.3
Isopropylether	3.88	1.368	0.145	324	30864.2	433	23094.7	7769.5	48.4
Ethyl ether	4.34	1.352	0.167	327	30581.1	437	22883.3	7697.7	46.3
THF	7.52	1.405	0.2096	326	30674.8	442	22624.4	8050.4	3.8
Dichloromethane	9.08	1.424	0.2183	326	30674.8	448	22321.4	8353.4	30.8
DMSO	47	1.478	0.2183	327	30581.1	456	21929.8	8651.2	25.6
Acetone	21.01	1.358	0.2847	328	30487.8	464	21551.7	8936.1	18.9
Acetonitrile	37.5	1.344	0.3053	329	30395.1	469	21321.9	9073.2	10.6

Table S6. Photophysical properties of PPINCN-Cz in different solvents.

Solvents	ε	n	f (ε,n)	λ_{ab} (nm)	ν_{ab} (cm^{-1})	λ_{flu} (nm)	ν_{flu} (cm^{-1})	ν_{ss} (cm^{-1})	Φ_{PL}
Hexane	1.88	1.37	0.0004	328	30487.8	395	25316.4	5171.3	62.0
Triethylamine	2.42	1.401	0.048	332	30120.5	403	24813.9	5306.6	59.3
Butyl ether	3.08	1.399	0.096	333	30030.1	408	24509.8	5520.2	52.8
Isopropyl ether	3.88	1.368	0.145	334	29940.1	412	24271.8	5668.3	43.1
Ethyl ether	4.34	1.352	0.167	336	29761.9	417	23980.8	5781.1	38.4
THF	7.52	1.405	0.2096	333	30030.1	420	23809.5	6220.5	32
Dichloromethane	9.08	1.424	0.2183	334	29940.1	422	23696.7	6243.4	28.3
DMSO	47	1.478	0.2183	332	30120.5	428	23364.5	6755.9	22.6
Acetone	21.01	1.358	0.2847	336	29761.9	434	22935.8	6826.1	17.8
Acetonitrile	37.5	1.344	0.3053	332	30120.5	436	22988.5	7131.9	6.9

Table S7. Computed integral of hole and electron overlap (S), distance between centroids of hole and electron (D, Å) and dipole moment (μ) for singlet and triplet states of PPINCN.

State	$\int h^+$	$\int e^-$	$\int T$	(S)	Centroid of hole (Å)			Centroid of electron (Å)			D (Å)	μ (a.u)
					x	y	z	x	y	Z		
S1	0.8244	0.7287	-0.0152	0.3846	-0.5583	1.1374	0.4357	-1.0278	1.2180	-0.0135	0.65	0.96
S2	0.8269	0.7294	-0.0117	0.2906	-0.6646	1.0144	0.4290	-1.7124	-0.2917	0.0565	1.71	2.52
S3	0.7997	0.6430	0.0097	0.2490	-0.8351	0.8621	0.3925	-0.4091	1.3998	-0.1515	0.87	1.19
S4	0.8579	0.7080	-0.0037	0.4988	-2.8068	-0.8770	-0.0420	-2.444	-0.8956	-0.1267	0.37	0.55
S5	0.7636	0.5982	-0.0037	0.3061	-1.1819	0.5734	0.3162	-0.4244	-0.1162	-0.2442	1.16	1.50
T1	0.7933	0.6633	-0.0210	0.4030	-0.5952	1.1036	0.4283	-0.3733	1.5856	0.1770	0.58	0.80
T2	0.7522	0.6101	-0.0054	0.4872	-2.9033	-0.9830	-0.0252	-3.2011	-1.3416	-0.1161	0.47	0.61
T3	0.6930	0.5502	0.0142	0.2428	-0.6646	1.0144	0.4290	-0.3484	1.8526	0.5668	0.90	1.06
T4	0.7959	0.5670	-0.0100	0.5128	3.6491	-0.7093	-0.0438	3.4568	-0.5505	-0.1042	0.25	0.33
T5	0.7038	0.5690	-0.0058	0.3125	-0.8039	1.1853	0.1920	-1.6229	0.2814	-0.2710	1.30	1.56

Table S8. Computed integral of hole and electron overlap (S), distance between centroids of hole and electron (D, Å) and dipole moment (μ) for singlet and triplet states of PPINCN-TPE.

State	$\int h^+$	$\int e^-$	$\int T$	(S)	Centroid of hole (Å)			Centroid of electron (Å)			D (Å)	μ (a.u)
					x	y	z	x	y	z		
S1	0.7897	0.6963	0.0223	0.3312	-6.5490	-1.3346	0.6804	-6.9642	-1.8725	0.2058	0.82	1.16
S2	0.7815	0.7004	-0.0150	0.2844	-6.5490	-1.3346	0.6804	-7.1396	-2.6407	0.2317	1.50	2.10
S3	0.6945	0.6618	-0.0078	0.1504	1.4818	9.2931	0.0320	0.8906	6.4816	-0.3226	2.89	3.70
S4	0.6826	0.6138	-0.0109	0.2061	1.5559	8.3578	-0.2752	1.0877	6.6595	-0.2670	1.76	2.15
S5	0.7825	0.6764	0.0031	0.2758	5.6625	-4.222	-.0.085	6.7277	-3.9191	0.1671	1.13	1.56
T1	0.7897	0.6963	0.0223	0.3312	-6.5490	-1.3346	0.6804	-6.9642	-1.8725	0.2058	0.82	1.16
T2	0.7815	0.7004	-0.0150	0.2844	-6.5490	-1.3346	0.6804	-7.1396	-2.6407	0.2317	1.50	2.10
T3	0.6945	0.6618	-0.0078	0.1504	1.4818	9.2931	0.0320	0.8906	6.4816	-0.3226	2.89	3.70
T4	0.6826	0.6138	-0.0109	0.2061	1.5559	8.3578	-0.2752	1.0877	6.6599	-0.2670	1.76	2.15
T5	0.7825	0.6764	0.0031	0.2758	5.6625	-4.2222	-0.0856	6.7277	-3.9191	0.1671	1.13	1.56

Table S9. Computed integral of hole and electron overlap (S), distance between centroids of hole and electron (D, Å) and dipole moment (μ) for singlet and triplet states of PPINCN-Cz.

State	$\int h^+$	$\int e^-$	$\int T$	(S)	Centroid of hole (Å)			Centroid of electron (Å)			D (Å)	μ (a.u)
					x	y	z	x	Y	z		
S1	0.8563	0.7538	0.0130	0.2469	6.8689	-0.7690	0.1273	6.1260	-2.3548	0.0177	1.75	2.66
S2	0.8134	0.6240	-0.0323	0.2898	6.8689	-0.7690	0.1273	6.6312	-1.0051	-0.1117	0.41	0.55
S3	0.8397	0.6591	0.0265	0.3020	6.8689	-0.7690	0.1273	5.8589	0.0515	-0.39690	1.39	1.97
S4	0.7960	0.6542	0.0060	0.1663	6.8689	-0.7690	0.1273	6.6560	-2.777	0.1329	2.02	2.76
S5	0.7910	0.5802	-0.0270	0.1715	6.8689	-0.7690	0.1273	4.7457	0.5031	-0.8584	2.66	3.45
T1	0.7811	0.6582	0.0354	0.3930	6.8689	-0.7690	0.1273	6.9866	-0.4236	0.2923	0.40	0.54
T2	0.6905	0.4575	-0.0208	0.2223	6.8689	-0.7690	0.1273	5.3322	-0.1778	-0.1946	1.67	1.82
T3	0.5229	0.3821	-0.0138	0.2910	5.4500	-0.6691	-0.1052	5.5153	-0.7088	-0.2448	0.15	0.13
T4	0.5229	0.3821	-0.0138	0.2910	5.4500	-0.6691	-0.1052	5.5153	-0.7088	-0.2448	0.15	0.13
T5	0.5443	0.4329	-0.0095	0.3065	1.4893	-1.0096	-0.1284	2.0142	-1.4774	-0.2912	0.71	0.66

Table S10. Computed RMSD of electron and hole, H index and t index for singlet and triplet states of PPINCN.

State	RMSD (Electron)				RMSD (Hole)				H index				t index			
	x	y	z	total	x	y	z	total	x	y	z	Total	x	y	z	Total
S1	2.283	2.291	1.172	3.440	2.297	1.573	1.091	2.990	2.290	1.932	1.131	2.990	-1.875	-1.394	-0.657	2.427
S2	2.783	2.671	1.206	4.041	2.297	1.573	1.091	2.990	2.540	2.122	1.148	3.503	-1.949	-0.816	-0.699	2.226
S3	2.474	2.984	0.914	3.982	1.891	1.944	0.884	2.853	2.182	2.464	0.899	3.412	-1.591	0.348	-0.544	1.717
S4	2.718	3.200	0.933	4.301	2.100	2.355	0.992	3.308	2.409	2.778	0.963	3.801	-1.940	-1.080	-0.955	2.417
S5	3.618	1.885	1.127	4.232	2.313	1.416	0.993	2.888	2.965	1.651	1.060	3.555	-1.900	-1.347	-0.807	2.465
T1	1.483	1.588	1.300	2.532	1.641	1.532	1.095	2.498	1.562	1.560	1.198	2.512	-1.340	1.078	-0.947	1.963
T2	2.638	1.965	0.740	3.371	2.975	2.033	0.835	3.699	2.806	1.999	0.787	3.534	-2.508	-1.640	-0.697	3.077
T3	1.545	1.657	1.551	2.745	1.831	1.522	1.072	2.611	1.688	1.589	1.311	2.663	-1.372	-0.751	-1.174	1.955
T4	2.664	2.069	0.818	3.471	2.683	2.016	0.833	3.458	2.674	2.042	0.826	3.464	-2.481	-1.884	-0.765	3.208
T5	2.430	2.514	1.055	3.652	1.916	1.903	1.220	2.963	2.173	2.208	1.138	3.300	-1.354	-1.304	-0.674	1.997

Table S11. Computed RMSD of electron and hole, H index and t index for singlet and triplet states of PPINCN-TPE.

State	RMSD (Electron)				RMSD (Hole)				H index				t index			
	x	y	z	total	x	y	z	total	x	y	z	Total	x	y	z	Total
S1	3.978	1.853	1.096	4.523	3.655	1.958	1.243	4.329	3.816	1.905	1.170	4.423	-3.637	-1.401	-0.761	3.971
S2	4.837	1.394	1.159	5.165	4.870	1.441	1.233	5.227	4.854	1.417	1.196	5.196	-4.241	-1.323	-1.095	4.575
S3	3.008	2.253	1.353	3.994	4.256	2.192	1.423	4.994	3.632	2.222	1.388	4.478	-2.948	-1.274	-1.084	3.390
S4	2.359	2.817	0.811	3.763	2.591	2.409	0.825	3.633	2.475	2.613	0.818	3.691	-2.086	-0.244	-0.794	2.246
S5	3.230	2.607	0.800	4.227	3.629	2.201	0.810	4.321	3.430	2.404	0.805	4.265	-2.973	-2.089	-0.796	3.720
T1	2.283	2.291	1.172	3.440	2.297	1.573	1.091	2.990	2.290	1.932	1.131	3.203	-1.875	-1.394	-0.657	2.427
T2	2.783	2.671	1.206	4.041	2.297	1.573	1.091	2.990	2.540	2.122	1.148	3.503	-1.949	-0.816	-0.699	2.226
T3	2.474	2.984	0.914	3.982	1.891	1.944	0.884	2.853	2.182	2.464	0.899	3.412	-1.591	0.348	-0.544	1.717
T4	2.718	3.200	0.933	4.301	2.100	2.355	0.992	3.308	2.409	2.778	0.963	3.801	-1.940	-1.080	-0.955	2.417
T5	3.618	1.885	1.127	4.232	2.313	1.416	0.993	2.888	2.965	1.651	1.060	3.555	-1.900	-1.347	-0.807	2.465

Table S12. Computed RMSD of electron and hole, H index and t index for singlet and triplet states of PPINCN-Cz.

State	RMSD (Electron)				RMSD (Hole)				H index				t index			
	x	y	z	total	x	y	z	total	x	y	z	Total	x	y	z	Total
S1	2.807	2,260	1.031	3.749	1.869	1.447	1.169	2.637	2.338	1.854	1.100	3.180	-1.595	-0.268	-0.991	1.897
S2	2.417	2.034	1.053	3.330	1.869	1.447	1.169	2.637	2.143	1.740	1.111	2.976	-1.905	-1.504	-0.872	2.579
S3	1.794	2.076	1.310	3.043	1.869	1.447	1.169	2.637	1.831	1.763	1.240	2.828	-0.821	-0.942	-0.743	1.454
S4	2.866	2.446	0.870	3.867	1.869	1.447	1.169	2.637	2.367	1.946	1.020	3.230	-2.154	0.062	-0.015	2.382
S5	2.660	2.244	1.093	3.648	1.869	1.447	1.169	2.637	2.264	1.845	1.131	3.132	-0.141	-0.573	-0.146	0.608
T1	2.070	1.745	1.230	2.974	1.869	1.447	1.169	2.637	1.969	1.596	1.200	2.804	-1.852	-1.250	-1.035	2.462
T2	2.024	1.788	1.192	2.952	1.869	1.447	1.169	2.637	1.946	1.617	1.181	2.792	-0.410	-1.026	-0.858	1.399
T3	3.256	2.724	1.214	4.415	3.783	2.442	1.165	4.651	3.520	2.583	1.190	4.525	-3.454	-2.543	-1.050	4.416
T4	3.256	2.724	4.415	3.783	2.442	1.165	1.165	4.651	3.520	2.583	1.190	4.525	-3.454	-2.543	-1.050	4.416
T5	3.769	2.502	0.837	4.601	4.165	2.707	0.953	5.057	3.967	2.604	0.895	4.829	-3.442	-2.137	-0.733	4.117

Table S13. Transferred charges (q_{CT}), barycentres of electron density loss (R_+) /gain (R-), distance between two barycenters (D_{CT}), dipole moment of CT (μ_{CT}), RMSD of +ve/-ve parts, CT indices (H & t) and overlap integral of C+/C- of PPINCN, PPINCN-TPE and PPINCN-Cz.

Blue emissive & Host materials	**R_+ (Å)**			**R- (Å)**			**D_{CT} (Å)**	**RMSD of +ve parts**	**RMSD of -ve parts**	**H / t indices (Å)**	**overlap integral of C+/ C-**
	x	y	z	x	y	z					
PPINCN	-0.573	-0.267	-0.068	-0.616	-0.258	-0.036	0.054	8.318	8.323	4.402/4.355	0.9977
PPINCN-TPE	-5.523	-0.043	-1.100	-0.942	-0.933	-0.799	4.677	13.148	5.321	4.885/2.199	0.5330
PPINCN-Cz	1.346	-0.091	-0.085	1.295	0.022	0.094	0.125	13.195	13.225	6.990/6.882	0.9998

References

[1] (a) M. J. Frisch, G. W. Trucks, H. B. Schlegel, G. E. Scuseria, M. A. Robb, J. R. Cheeseman, G. Scalmani, V. Barone, B. Mennucci, G. A. Petersson, H. Nakatsuji, M. Caricato, X. Li, H. P. Hratchian, A. F. Izmaylov, J. Bloino, G. Zheng, J. L. Sonnenberg, M. Hada, M. Ehara, K. Toyota, R. Fukuda, J. Hasegawa, M. Ishida, T. Nakajima, Y. Honda, O. Kitao, H. Nakai, T. Vreven, J. A. Montgomery, J. E. Peralta, F. Ogliaro, M. Bearpark, J. J. Heyd, E. Brothers, K. N. Kudin, V. N. Staroverov, R. Kobayashi, J. Normand, K. Raghavachari, A. Rendell, J. C. Burant, S. S. Iyengar, J. Tomasi, M. Cossi, N. Rega, J. M. Millam, M. Klene, J. E. Knox, J. B. Cross, V. Bakken, C. Adamo, J. Jaramillo, R. Gomperts, R. E. Stratmann, O. Yazyev, A. J. Austin, R. Cammi, C. Pomelli, J. W. Ochterski, R. L. Martin, K. Morokuma, V. G. Zakrzewski, G. A. Voth, P. Salvador, J. J. Dannenberg, S. Dapprich, A. D. Daniels, O. Farkas, J. B. Foresman, J. V. Ortiz, J. Cioslowski, D. J. Fox, *Gaussian, Inc., Wallingford CT (Revision A.**02**), Gaussian, Inc., Wallingford., CT*. 2009.

[2] J. Jayabharathi, R. Ramyaa, V. Thanikachalam, P. Jeeva and E. Sarojpurani, *RSC Adv*., 2019, **9**, 2948-2966.

[3] H. Liu, Q. Bai, L. Ya, H. Zhan, H. Xu, S. Zhang, W. Li, Y. Gao, J. Li, P. Lu, H. Wang, B. Yang and Y. Ma, *Chem. Sci.,* 2015, **6**, 3797-3804.

[4] Z. Wang, Y. Feng, H. Li, Z. Gao, X. Zhang, P. Lu, P. Chen, Y. Mab and S. Liu, *Phys. Chem. Chem. Phys.,* 2014, **16**, 10837-10843.

[5] Y. F. Chang, H. F. Meng, G. L. Fan, K. T. Wong, H. W. Zan, H. W. Lin, H. L. Huang and S. F. Horn, *Org. Electron.*, 2016, **29**, 99-106.

[6] Y. Zhang, T. Wai, N. F. Lua, Q. X. Tong, S. L. Lai, M. Y. Chan, H. L. Kwong and C. S. Lee, *Dyes Pigm.*, 2013, **98**, 190-194.

[7] G. Li, J. Zhao, D. Zhang, J. Zhu, Z. Shi, S. Tao, Feng Lu and Q. Tong, *New J. Chem.,* 2017, **41**, 5191-5197.

[8] S. Liu, F. He, H. Wang, H. Xu, C. Wang, F. Li and Y. Ma, *J. Mater. Chem.,* 2008, **18**, 4802-4807.

[9] S. Kim, B. Sanyoto, W. T. Park, S. Kim, S. Mandal, J. C. Lim, Y. Y. Noh and J. H. Kim, *Adv. Mater.*, 2016, **28**, 10149-10154.

[10] X. L. Li, X. Ouyang, D. Chen, X. Cai, M. Liu, Z. Ge, Y. Cao and S. J. Su, *Nanotechnol.,* 2016, **27**, 124001-124011.